Pergamon

Geochimica et Cosmochimica Acta, Vol. 64, No. 22, pp. 3853–3869, 2000

0016-7037/00 $20.00 + .00

PII S0016-7037(00)00471-3

Synthetic fluid inclusions: XVI. PVTX properties in the system H_2O-NaCl-CO_2 at elevated temperatures, pressures, and salinities

C. SCHMIDT*,† and R. J. BODNAR

Fluids Research Laboratory, Department of Geological Sciences, Virginia Tech, Blacksburg, VA 24061-0420, USA

(*Received September* 27, 1999; *accepted in revised form May* 31, 2000)

Abstract—The ternary system H_2O-NaCl-CO_2 is one of the most important fluid systems in geochemistry and petrology. However, there is little information on the phase equilibrium and PVT properties in this system at salinities above 6 wt.% NaCl. In this study, PVTX data were obtained experimentally by using the synthetic fluid inclusion technique in conjunction with conventional microthermometry and a hydrothermal diamond–anvil cell.

Solvi (liquid-vapor boundaries) and lines of equal homogenization temperature (approximating lines of constant density) were determined for pressures between about 100 and 500 MPa, temperatures of 300°C to 800°C, and compositions up to 40 wt.% NaCl and 20 mol.% CO_2, both relative to water. Critical temperatures were obtained for ternary compositions $\leq$ 20 wt.% NaCl and $\leq$ 20 mol.% CO_2, both relative to water.

For a constant homogenization temperature, the dP/dT slopes of lines of equal homogenization temperature become steeper along pseudobinaries with both increasing carbon dioxide concentration and increasing NaCl. At constant salinity, the high-pressure portion of the solvus shifts to higher pressures and temperatures with increasing CO_2 concentration. Addition of carbon dioxide causes the critical point to migrate towards higher pressures and slightly lower temperatures. For concentrations less than 20 wt.% NaCl and less than 20 mol.% CO_2, the main effect of an increase in salinity at a fixed H_2O/CO_2 ratio is a sharp rise in the critical temperature, coupled with a moderate shift of the critical point towards higher pressures. The addition of CO_2 and NaCl causes the solvus to migrate to high temperatures and pressures, reaching granulite–facies conditions for moderate to high concentrations of CO_2 and NaCl. The results of this study are combined with literature data to construct P-T sections, with lines of constant homogenization temperature, for various compositions in the H_2O-NaCl-CO_2 ternary, and the results are compared with results predicted by a recently published equation of state.

1. INTRODUCTION

1.1. Previous Studies

With the increased application of fluid inclusions in petrologic studies during the last four decades, it became evident that many inclusions from a variety of crustal environments are approximated by the ternary system H_2O-NaCl-CO_2. Such fluids have been observed in contact metamorphic, greenschist, and amphibolite facies metamorphic rocks, granitoids, pegmatites, alkaline igneous rocks, carbonatites, geothermal brines, and a wide variety of hydrothermal deposits (Roedder, 1984; Labotka, 1991). Some properties of this ternary system have substantial petrologic and geochemical implications. These include (1) the extension of two-phase (immiscibility) conditions to higher pressures and temperatures (compared to either of the binary systems H_2O-NaCl or H_2O-CO_2) and (2) the effect on mineral equilibria of lowering of the water activity by the addition of both an electrolyte and a nonpolar volatile component (Bowers and Helgeson, 1983a,b). Furthermore, the accurate interpretation of naturally occurring H_2O-NaCl-CO_2 fluid inclusions requires volumetric and phase equilibrium data over the range of PTX conditions found in crustal environments.

Critical properties, solvus location, and salt solubility in water-volatile-electrolyte systems such as H_2O-NaCl-CO_2 are also relevant to supercritical water oxidation technology for the treatment of hazardous organic wastes. PVTX data are needed to optimize operating conditions in supercritical water oxidation reactors and for the design of salt separation loops (Shaw et al., 1991; Tester et al., 1992; Bodnar, 1995). Phase equilibrium data for the H_2O-NaCl-CO_2 system are also relevant to the desalination of seawater (Bozzo et al., 1975) and storage of nuclear waste in evaporites (Roedder, 1984 and references therein).

Determination of the solubility of CO_2 in H_2O-NaCl mixtures was the main goal of early work conducted in this ternary system. Ellis and Golding (1963) determined the solubility of CO_2 in sodium chloride solutions up to 2 molal NaCl and 330°C. Takenouchi and Kennedy (1965) extended these data to 20 wt.% NaCl, 140 MPa, and 450°C. [Note at this point that throughout the following text, figures, and tables, concentration units of mol fractions refer to sodium chloride and carbon dioxide concentrations in a ternary H_2O-NaCl-CO_2 mixture. Use of wt.% or mol.% denotes the concentration of a substance relative to water, e.g., 20 wt.% NaCl = (20 g NaCl · 100%)/(20 g NaCl + 80 g H_2O)]. Drummond (1981) studied CO_2 solubility in NaCl solutions up to 6 molal between 25°C and 400°C. Malinin and Savelyeva (1972), Malinin and Kurovskaya (1975), and Yasunishi and Yoshida (1979) determined carbon dioxide solubilities in aqueous sodium chloride solutions up to 6 molal and at temperatures between 15°C and 150°C. These studies show that addition of NaCl results

* Author to whom correspondence should be addressed (hokie@gfz-postdam.de).
† *Present address:* GeoForschungsZentrum Potsdam, Telegrafenberg D329, 14473 Potsdam, Germany.

in a significant reduction of CO_2 solubility ("salting-out" effect).

Compared to phase equilibrium data, volumetric data for the H_2O-NaCl-CO_2 system are more limited, and are generally restricted to low salinities. The synthetic fluid inclusion technique was used to determine solvus locations and lines of constant homogenization temperature (approximating isochores) (Kotelnikov and Kotelnikova, 1990; Frantz et al., 1992; Johnson, 1991; Johnson, 1992; Shmulovich and Plyasunova, 1993; Schmidt et al., 1995; Gibert et al., 1998; Shmulovich and Graham, 1999). Joyce and Holloway (1993) and Blencoe et al. (1996) obtained activity-mole fraction relations of water in H_2O-CO_2-NaCl mixtures directly by reacting fluid samples in an internally heated pressure vessel at constant pressure, temperature, and hydrogen fugacity and measuring the shift in mole fraction H_2O after quenching.

PTX conditions of critical points are known for limited ranges along the H_2O-NaCl and H_2O-CO_2 binaries (Sourirajan and Kennedy, 1962; Tödheide and Franck, 1963; Takenouchi and Kennedy, 1964; Knight and Bodnar, 1989; Sterner and Bodnar, 1991). Frantz et al. (1992) reported an approximate location of the critical point for one ternary mixture. The most extensive experimental dataset for ternary compositions was obtained by Gehrig (1980). Using a high-pressure variable-volume autoclave, he determined molar volumes and immiscibility limits along the (H_2O + 6 wt.% NaCl)-CO_2 pseudobinary up to 300 MPa and temperatures to 560°C. He also obtained less detailed volumetric and solvus data for the (H_2O + 10 and 20 wt.% NaCl)-CO_2 pseudobinaries at low carbon dioxide concentrations (up to 7 mol.% CO_2 at 20 wt.% NaCl and up to 12 mol.% CO_2 at 10 wt.% NaCl). The data of Gehrig (1980) are the main empirical basis of the modified Redlich–Kwong equation of state by Bowers and Helgeson (1983a) and the equation of state of Duan et al. (1995), which uses the approach of Anderko and Pitzer (1993). Brown and Lamb (1989) modeled isochore positions of H_2O-NaCl-CO_2 mixtures by linear interpolation of H_2O-NaCl and CO_2 isochores.

Low-temperature phase equilibria involving clathrate were studied by Chen (1972); Bozzo et al. (1975); and Diamond (1992, 1994). Barton and Chou (1993) calculated the vapor-saturated liquidus surface in the H_2O-rich corner of the ternary. Fewer data are available for the liquidi at higher NaCl and CO_2 concentrations (Chou, 1988; Schmidt et al., 1995).

1.2. High-Temperature Phase Behavior in the System H_2O-NaCl-CO_2

A schematic phase diagram of the system H_2O-NaCl-CO_2 at elevated P-T conditions is shown in Figure 1. The diagram includes all the various PVTX elements examined in this study. The ternary shows topological similarities to the binary H_2O-CO_2 with respect to the general shape of the immiscibility region (c.f., Takenouchi and Kennedy, 1964; Tödheide and Franck, 1963). An important difference that has significant implications for understanding fluid behavior in high temperature and pressure environments is the expansion of the immiscibility field towards higher pressures and temperatures with addition of NaCl. The liquid-vapor curve (solvus) defines the limits of the two-phase liquid-vapor region (immiscibility field) (L + V; Fig. 1). The solvus consists of the bubble-point curve

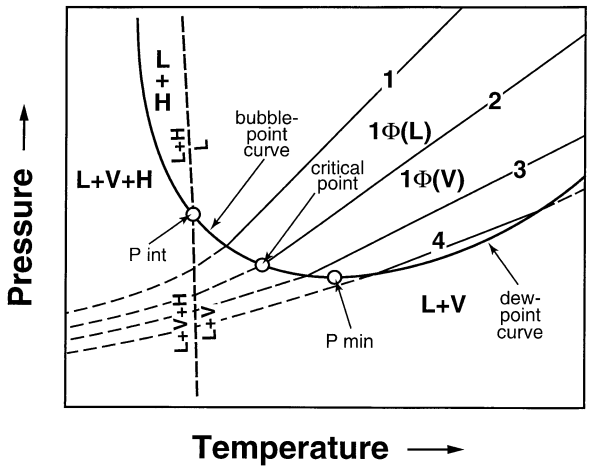

Fig. 1. Schematic topology of the system water-sodium chloride–carbon dioxide at high P and T and applicable to compositions in the range of about 30 to 40 wt.% NaCl and approximately 1 to 5 mol.% CO_2. Heavy lines indicate boundaries of phase stability fields: solvus (heavy solid line), liquidus (heavy dashed line). 1Φ(L) = one-phase region, fluid density above the critical density (homogenization to liquid); 1Φ(V) = one-phase region, fluid density below the critical density (homogenization to vapor); L + V = coexisting liquid and vapor; L + H = coexisting liquid and halite; L + V + H = coexisting liquid, vapor, and halite. P min = local pressure minimum of the solvus; P int = point of intersection of liquidus with the liquid-vapor curve. Four different isochores (1 to 4) are depicted as thin lines. Within the one-phase field these lines are solid; within the two- or three-phase fields these lines are dashed. See text for more details.

(bulk density of the fluid greater than the critical density) and the dew-point curve (bulk density of the fluid less than the critical density). For some compositions in the ternary, the solvus displays a local pressure minimum at moderate to high temperatures (P min; Fig. 1). At temperatures below the temperature of the pressure minimum (towards high fluid densities), the solvus pressure becomes increasingly less dependent on temperature for most compositions (Gehrig, 1980). At temperatures above the temperature of the pressure minimum, the solvus pressure increases gradually (Fig. 1). Although there are no experimental data, by analogy with the H_2O-NaCl binary system, a vapor + halite field should exist at low pressures (below the L + V field) due to the reduced solubility of NaCl in the vapor.

For compositions containing greater than about 25 to 30 wt.% NaCl (relative to H_2O), the liquid and liquid + vapor fields are truncated at low temperature by the halite liquidus (L + H; Fig. 1). At pressures above the bubble-point curve, the liquidus separates the high temperature single-phase field (L; Fig. 1) from the lower temperature region in which an NaCl-saturated liquid coexists with halite (L + H; Fig. 1). At pressures below the bubble-point pressure, the liquidus separates a liquid + vapor field at higher temperature from a lower temperature three-phase field in which liquid + vapor + halite coexist (L + V + H; Fig. 1). The intersection of the liquidus with the bubble-point curve (P int; Fig. 1) is equivalent to the intersection of the halite liquidus with the liquid-vapor curve in the H_2O-NaCl binary (c.f., Bodnar, 1994).

The slopes (dP/dT) of the isochores (or iso-Th lines) in the

H_2O-NaCl-CO_2 system are steep for lower homogenization temperatures (higher densities), and flatten as Th increases or density decreases. Thus, the slope of the isochore labeled "1" (Fig. 1), representing an H_2O-NaCl-CO_2 inclusion that homogenizes to the liquid phase, is steeper than that of an inclusion with the same composition but a lower density and which homogenizes to the vapor phase (isochore "3"; Fig. 1). The P-T path followed by an inclusion that homogenizes by critical behavior, as described in more detail below, must intersect the solvus at the critical point. Extrapolation of this isochore (isochore "2"; Fig. 1) into the one-phase region serves to divide fluids with "liquid-like" properties at pressures above the isochore, from fluids with "vapor-like" properties at pressures below the critical isochore. The pressure minimum on the solvus, described above, offers some unusual possibilities for isochoric P-T paths. For example, synthetic fluid inclusion experiments of Frantz et al. (1992) suggest that some isochores in the H_2O-NaCl-CO_2 system may intersect the same phase boundary twice (Fig. 1, isochore "4"). Diamond (1996) later showed that this behavior is theoretically possible. If similar behavior occurs for some PTX trapping conditions in the H_2O-NaCl-CO_2 ternary, the "first" (lowest) homogenization temperature may not provide a good approximation of the formation temperature of the host sample. However, direct experimental confirmation of the results of Frantz et al. (1992), i.e. observation of high-temperature heterogenization of a previously homogenized fluid inclusion, is still lacking.

In this study, we used the synthetic fluid inclusion technique to extend data for PVTX properties of the H_2O-NaCl-CO_2 system to 800°C, 500 MPa, and 40 wt.% NaCl relative to water. Data obtained include solvus positions, lines of constant homogenization temperature (iso-Th lines), and critical properties, along with estimates of liquidus locations.

2. EXPERIMENTAL TECHNIQUES, SOURCES OF ERROR, AND DATA REDUCTION

2.1. Fluid Inclusion Synthesis

All data reported in this study were obtained from synthetic fluid inclusions in quartz. During the last 15 years, the synthetic fluid inclusion technique has been established as a proven method for the determination of phase equilibria and volumetric properties in aqueous fluid systems containing salt and volatiles. The method is particularly useful for the study of high-salinity fluids at elevated temperature and pressure, because it avoids corrosion and fluid sampling problems associated with many conventional techniques. Details, uses and limitations of the synthetic fluid inclusion technique were described by Bodnar and Sterner (1987), Sterner and Bodnar (1984, 1991), and Sterner (1992); the reader may refer to these papers for specific aspects outside the focus of this study.

Most experiments were conducted at the following six bulk fluid compositions along three pseudobinaries in the system water-sodium chloride-carbon dioxide:

1) (H_2O + 6 wt.% NaCl)-CO_2, having carbon dioxide concentrations of 10 mol.% or 20 mol.% CO_2 relative to water,
2) (H_2O + 20 wt.% NaCl)-CO_2, including carbon dioxide concentrations of 10 or 20 mol.% CO_2 relative to water, and
3) (H_2O + 40 wt.% NaCl)-CO_2, having carbon dioxide concentrations of 5 or 10 mol.% carbon dioxide relative to water.

Starting materials to generate the required fluid composition and a prefractured quartz core were loaded into platinum capsules, which were then sealed with an arc welder. If the fluid contained 6 or 20 wt.% NaCl, silver oxalate ($Ag_2C_2O_4$) (used as the carbon dioxide source) was loaded first, followed by either a 6 or 20 wt.% sodium chloride standard solution. The amount of solution added was calculated to give the desired H_2O/CO_2 ratio after silver oxalate decomposition. For 40 wt.% NaCl compositions, dried halite (NaCl) was added to the capsule first, followed by silver oxalate, and then deionized, distilled water in the amount required to generate a salinity of 40 $\pm$ 0.1 wt.% sodium chloride. The actual carbon dioxide yield of the silver oxalate was determined previously by decomposing a known amount of $Ag_2C_2O_4$ in sealed platinum capsules and measuring the weight loss after piercing the capsules (Sterner and Bodnar, 1991).

The sealed capsules and filler rods (to reduce thermal gradients) were loaded into horizontal cold-seal pressure vessels and run at the pressure and temperature of interest (200–500 MPa and 300°C–700°C). To minimize damage to the capsules during the rapid (explosive) silver oxalate decomposition, the vessels were pressurized to 50–70 MPa before heating. This pressure was maintained until the silver oxalate in the capsules decomposed at a temperature of about 200° to 250°C (Sterner and Bodnar, 1991). During heating to the final experimental temperature, the pressure in the vessels was gradually increased and (at temperatures above 300° to 400°C) repeatedly cycled over a range of several tens to a few hundred MPa to minimize premature fracture healing and promote mixing of the fluid in the capsules (Bodnar and Sterner, 1987). During cycling, the pressure was at least about 100 MPa above the expected solvus pressure in order to avoid entering the two-phase field. Once the experimental temperature was reached, the pressure was cycled several times between the experimental pressure and 100 to 200 MPa above this pressure. An internally heated pressure vessel (IHPV) with argon as the pressure medium was used for the 800°C experiments. Owing to the dependence of quartz solubility (and thus fracture healing rates) on temperature, run durations varied with experimental temperature as follows: about 8 weeks for a formation temperature [Tf] of 300°C, approximately 4 weeks at Tf = 400°C, 2 weeks at Tf = 500°C, 4 to 6 d for Tf between 600° and 700°C, and 1 to 3 d if Tf was 800°C. During that time, synthetic inclusions formed by entrapment of fluid in healed fractures or, at temperatures $\geq$500°C, by dissolution and reprecipitation of quartz as an overgrowth on the core. After completion of the experiments, the pressure vessels were cooled approximately isochorically.

After the run, the capsules were dried, wrapped in tissue, equilibrated with the atmospheric moisture, weighed and then punctured. The weight loss within the first few seconds after puncturing, which is predominantly caused by loss of CO_2, was used to confirm that the actual amount of CO_2 in the capsules corresponded to the amount expected from the mass of silver oxalate loaded. Although this technique can be relatively inaccurate for CO_2 + water solutions (Sterner and Bodnar, 1991), the deviation was mostly within 2% of the expected amount of CO_2. Fluid compositions along the 40 wt.% NaCl pseudobinary tended to show somewhat lower (by about 1 or 2%) apparent CO_2 yields than samples containing 6 wt.% NaCl relative to water. This apparent loss of carbon dioxide can probably be attributed to the formation of HCO_3^- in the aqueous phase during the synthesis and subsequent precipitation of nahcolite ($NaHCO_3$) during the quench. Finally, the quartz cores were removed from the capsules, cut into disks, polished on both sides, and examined using petrographic and microthermometric techniques. Additionally, some samples were analyzed using Raman spectroscopy and SEM-EDS.

At room temperature, all synthesized H_2O-NaCl-CO_2 inclusions contained aqueous brine and a CO_2-rich vapor phase. Additionally, a liquid CO_2 phase was observed in high density inclusions. Halite was present in inclusions that had a salinity above NaCl saturation. A small opaque phase commonly occurred in inclusions and adjacent healed fractures in the quartz and was identified as elemental silver using SEM-EDS and reflected light microscopy. A strongly birefringent phase was detected in some inclusions in a number of samples formed at temperatures $\geq$ 550°C, run pressures $\geq$ 400 MPa, and salinities of 20 or 40 wt.% NaCl. This phase was identified as nahcolite ($NaHCO_3$) using Raman spectroscopy. When nahcolite occurred, it occupied a small volume fraction of the inclusions. Chlorargyrite was only observed in inclusions synthesized using an IHPV. The identity of this phase was verified by exposing it to UV radiation.

2.2. Microthermometry

For inclusions having compositions along the 6 wt.% and 20 wt.% NaCl pseudobinaries, four phase transition temperatures were determined:

1) The melting temperature of solid carbon dioxide in the presence of CO_2 hydrate, NaCl hydrate, CO_2 liquid, and vapor [Tm(CO_2)],
2) The dissociation temperature of CO_2 hydrate in equilibrium with aqueous brine, and liquid and vapor carbon dioxide [Tm(CLA)],
3) The homogenization temperature of the carbonic liquid and vapor phases [Th(CO_2)], and
4) The temperature of total homogenization of CO_2-rich vapor and aqueous liquid to a single homogeneous phase [Th(L-V)].

The CO_2 triple point (−56.6°C) was used to confirm the purity of the carbon dioxide in the inclusions. The inclusion salinity was calculated from the clathrate dissociation temperature Tm(CLA) using the equations of Darling (1991) and Diamond (1992). The density of the carbonic phase at low temperature was obtained from Th(CO_2) (Lowry and Erickson, 1927) assuming that this phase consists of pure carbon dioxide. Furthermore, the consistency of homogenization temperatures of the carbonic phases (when the carbon dioxide homogenized to the liquid) was applied as an additional test for the homogeneity of the fluid samples at the experimental PTX conditions. Lines of equal homogenization temperature and some solvi were calculated based on the measured total homogenization temperatures as described below. If the inclusions contained 40 wt.% sodium chloride relative to water, the temperature of halite dissolution [Tm halite] in the presence of aqueous liquid and CO_2-rich vapor was measured instead of the clathrate dissociation temperature and was used to estimate liquidus positions.

A Fluid Inc adapted USGS-type gas-flow heating/freezing stage (Werre et al., 1979) was used for microthermometric measurements of phase transitions at one atmosphere external pressure. The thermocouple was routinely calibrated against the CO_2 triple point (−56.6°C), the clathrate dissociation temperature of a H_2O-CO_2 inclusion (10.0°C), and the triple point (0.0°C) and critical point of water (374.1°C) using synthetic fluid inclusion standards (Sterner and Bodnar, 1984). The α-β transition temperature of the host quartz (571°C) was used to check the accuracy of homogenization temperature measurements above about 470°C.

In conventional fluid inclusion studies, it is possible to work with inclusions as small as 2 to 3 μm in diameter. With such small inclusions, it is usually necessary to use a "cycling technique" to determine temperatures of various phase changes, as the actual phase changes (i.e., bubble disappearance, ice melting, etc.) are often not discernible. In the present study, the cycling technique could not be used to determine Th because the vapor bubble renucleates within a few degrees Celsius of Th(L-V) during cooling, precluding use of the bubble nucleation hysteresis as a means of determining whether or not homogenization had occurred. Thus, homogenization temperatures could only be determined accurately for inclusions larger than about 10 μm in diameter, i.e., large enough to allow the bubble disappearance to be observed. However, using only relatively large inclusions introduced another problem. H_2O-NaCl-CO_2 inclusions often generate high internal pressures during heating to homogenization, causing the host mineral to stretch or decrepitate before Th is reached. And, it is well known that the maximum internal pressure that an inclusion in quartz can maintain without stretching or decrepitating is related to the inclusion size, with small inclusions being able to withstand higher pressures than larger inclusions. Thus, although a 2 μm inclusion can maintain an internal pressure of about 300 MPa without decrepitating, a 10 μm inclusion will decrepitate with about 160 MPa of internal pressure, and a 20 μm inclusion requires only about 120 MPa (Bodnar et al., 1989). In this study, inclusions ≥10 μm in diameter and having salinities ≥20 wt.% NaCl generated internal pressures high enough to cause decrepitation before the homogenization temperature was reached, and prevented determination of Th(L-V) using a one-atmosphere gas-flow heating stage. Therefore, a hydrothermal diamond–anvil cell (HDAC) (Bassett et al., 1993; Chou et al., 1994; Schmidt et al., 1998) was used as a pressurized fluid inclusion stage to exert a confining pressure on the sample during heating for these inclusions.

The HDAC thermocouples were calibrated at the one-atmosphere melting points of azobenzene (68°C), sodium nitrate (306.8°C), and sodium chloride (801°C). The sample chamber of the hydrothermal diamond-anvil cell was loaded with water and a chip of quartz containing synthetic fluid inclusions. The water served as the confining pressure medium. Th(L-V) and, if halite was present, Tm halite were measured for samples having bulk compositions of H_2O + 40 wt.% NaCl + 10 mol.% CO_2 and H_2O + 20 wt.% NaCl + 20 mol.% CO_2. The pressure in the chamber at the phase transition temperature was calculated from the density of the pressure medium (water) using the equation of Haar et al. (1984). The homogenization temperature of inclusions determined using the HDAC depends on the confining pressure (Schmidt et al., 1998). Thus, Th(L-V) was measured for each sample at different (but known) confining pressures and normalized to a confining pressure equal to the estimated solvus pressure to correct for the effect of elastic volume change of the inclusion host quartz. The solvus pressure for these compositions was estimated from the limits of immiscibility as determined from petrographic and low-temperature microthermometric data. Details of the procedure used for the HDAC measurements are described by Schmidt et al. (1998).

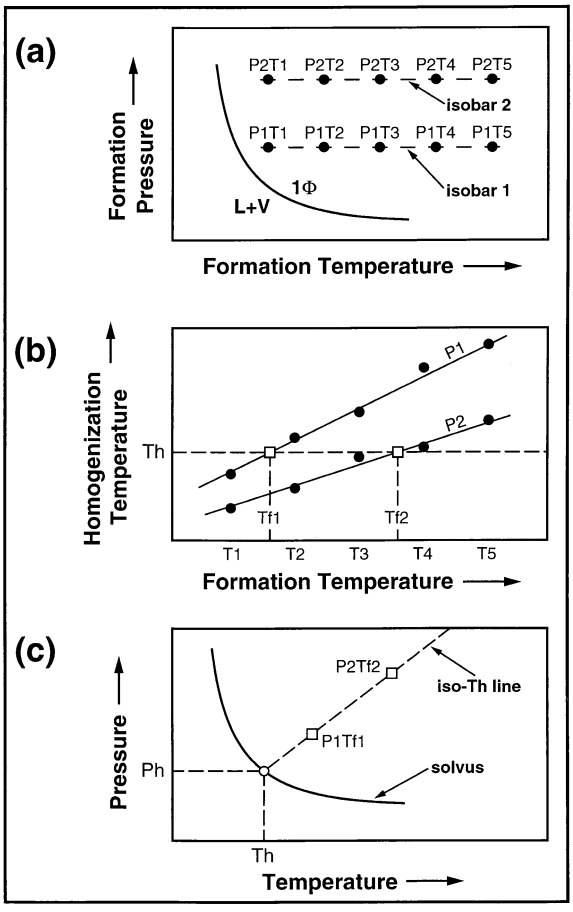

Fig. 2. Schematic diagrams illustrating the procedure for determining iso-Th lines (a and b) and the "slope–intercept" technique to locate the liquid-vapor curve (c). T = temperature; P = formation pressure; Tf = formation temperature; Th = total homogenization temperature; Ph = total homogenization pressure; L + V = liquid-vapor field; 1Φ = one-phase field.

2.3. Location of Solvi, Lines of Equal Homogenization Temperature, and Critical Points

Iso-Th lines corresponding to a given Th were determined as follows. Fluid inclusions were synthesized at different temperatures [Tf] along at least two isobars [Pf] (Fig. 2a) and the total homogenization

temperature [Th(L-V)] was determined for each sample. Then, the formation temperatures of samples that formed in the one-phase field were regressed as linear (and in a few cases quadratic) functions of the average Th(L-V) for each isobar (Fig. 2b). At high fluid densities, we found little dependence of Th(L-V) on Tf and Pf because the solvus pressure shows a large increase over a small temperature interval, i.e., the solvus is nearly parallel to the pressure axis. This results in a higher uncertainty in the slopes of the calculated iso-Th lines because the error in determining Th(L-V) becomes much more significant in this P-T region. Therefore, such data were excluded from the regressions to improve the quality of the fits. The regression equations for each isobar were then solved for specific Th(L-V) values to determine (Tf, Pf) points corresponding to those homogenization temperatures (Fig. 2b). These (Tf, Pf) points were then fitted by a straight line referred to as an iso-Th line (line of constant homogenization temperature) (Fig. 2c). The procedure was repeated for a range of Th(L-V) values and the slopes of the calculated iso-Th lines were then smoothed as a function of Th(L-V).

Previous experimental studies (e.g., Gehrig, 1980) showed that deviations of isochores from linearity in the one-phase field are normally small over the range of pressures and temperatures of this study and within the error associated with the experimental technique. Therefore, linear fits to (Tf, Pf) points corresponding to the same Th(L-V) were assumed to be sufficient to determine the dP/dT slopes of the iso-Th lines. This assumption simplifies the data reduction and greatly reduces the number of required experiments. However, it should be kept in mind that a linear model is only a first approximation to locate iso-Th lines because the molar volume of the host mineral will rarely remain constant along an inclusion isochore. Therefore, the volume of the fluid inclusion usually changes slightly between its temperature and pressure of formation and the temperature and pressure of homogenization. Elastic effects that cause the homogenization temperature to be dependent on the difference between internal and confining pressure on the inclusion are small and are taken into account using the procedure described by Schmidt et al. (1998).

Although iso-Th lines are not identical to isochores, there is usually little difference between the slope of an iso-Th line and that of an isochore having the same molar volume at Th(L-V). If the molar volume is known at any P-T point of an iso-Th line, the iso-Th lines can be converted to isochores by correcting for the slightly non-isochoric behavior of the quartz host using the equation of state for α- and β-quartz of Hosieni et al. (1985) as described by Bodnar and Sterner (1985) and Sterner and Bodnar (1991).

Two different techniques were applied to obtain solvus pressures: (1) the "slope-intercept" technique (Sterner and Bodnar, 1991) and (2) delineation of the liquid + vapor field in P-T space using petrographic and microthermometric evidence (Bodnar et al., 1985). To calculate the pressure of the liquid-vapor curve using the "slope-intercept" approach, individual iso-Th lines were extrapolated to their corresponding total homogenization temperatures (Fig. 2c). This method has the advantage that the fluid composition is known accurately because the fluid inclusions are trapped in the single-phase field and thus their composition is identical to the known composition loaded into the capsule. The "slope-intercept" technique has been applied successfully to determine critical points and liquid-vapor curves in the systems H_2O-NaCl (Knight and Bodnar, 1989; Bodnar and Vityk, 1994), H_2O-CO_2 (Sterner and Bodnar, 1991), and H_2O-NaCl-CO_2 (Schmidt et al., 1995). However, the error in calculated solvus pressure associated with this method can be very large if iso-Th line slopes are steep and intersect a portion of the liquid-vapor curve that is almost independent of temperature. (Similarly, a large temperature error can result if the iso-Th lines are shallow and intersect a portion of the solvus that is almost pressure independent.) Therefore, an additional approach was used in conjunction with the "slope-intercept" technique to locate the immiscibility field. This technique brackets the formation pressures and temperatures of the experiments along isotherms or isobars. Samples that show a large scatter in phase ratios, salinity, density of the CO_2-rich phase, and Th(L-V) data, and record total homogenization temperatures greater than or equal to the formation temperature of the sample indicate the presence of an unmixed fluid at the formation conditions (c.f., Bodnar et al., 1985). Samples that trapped a single phase, homogeneous fluid are characterized by fluid inclusions displaying consistent phase ratios and total homogenization temperatures (which are less than the formation temperature).

The critical iso-Th line for a specific composition is obtained using a technique similar to the previously described procedures. Fluid inclusions having a bulk density higher than the critical density homogenize by shrinking and disappearance of the vapor bubble at the homogenization temperature, whereas fluid inclusions with bulk densities lower than the critical density homogenize by expansion of the vapor phase to fill the inclusion. If fluid inclusions of critical specific volume (density) are heated, the densities and the compositions of the liquid and vapor phases approach each other as the homogenization temperature is approached; such inclusions homogenize by fading and disappearance of the meniscus between liquid and vapor at the critical point. Along a given isobar, formation temperatures that bracket inclusions that homogenize by shrinking of the vapor bubble and those that homogenize by expansion of the vapor bubble were identified. Inclusions were then synthesized at increasingly smaller temperature steps within this range until inclusions homogenizing by critical behavior were obtained. The critical point pressure was then calculated by intersection of the critical iso-Th line with the measured critical temperature, which can usually be determined with an accuracy of about ± 5°C or better for temperatures below 500°C.

2.4. Experimental Errors

2.4.1. Compositional errors

The uncertainty associated with weighing starting materials during capsule loading is ≤ 0.0001 g, which corresponds to a 0.2% error for an average of 0.05 g per loaded substance. A somewhat larger, but known, compositional error can result from the difficulty of accurately adjusting the weights of solid NaCl and silver oxalate during capsule loading. The carbon dioxide yield of the silver oxalate batch used for all runs was checked frequently by decomposing known amounts of $Ag_2C_2O_4$ in a sealed Pt capsule and determining the weight loss after piercing; the yield averaged between 99.6 and 99.3%. The uncertainty in CO_2 yield of silver oxalate as determined from weight loss measurements before loading of H_2O-NaCl-CO_2 capsules was approximately 0.5%. During the course of this investigation, the CO_2 yield of the silver oxalate was maintained by storing the silver oxalate in vacuum and minimizing exposure to light and atmospheric moisture.

Measurements of the melting temperature of solid carbon dioxide in equilibrium with vapor and liquid CO_2 [$Tm(CO_2)$] were used to determine the purity of the carbon dioxide in the synthesized inclusions. The $Tm(CO_2)$ of most samples was within ± 0.2°C (the uncertainty of the temperature measurements) of the triple point temperature of pure carbon dioxide (-56.6°C). Inclusions in some samples showed a slight depression of the CO_2 triple point down to -57.4°C indicating the presence of small amounts of another gas. In a few of these inclusions, traces of methane were identified using Raman spectroscopy. This occasional contamination should not have a large effect on the determined phase equilibria due to the relatively low concentrations. Samples with lowered $Tm(CO_2)$ and detectable methane generally had run durations of several weeks and formation temperatures of 400°C and 450°C.

Due to the presence of silica from the host mineral and silver from the decomposition of silver oxalate, the fluid system in the capsules is more accurately described as H_2O-CO_2-NaCl-SiO_2-Ag. To our knowledge, no data are available for the solubility of quartz in H_2O-CO_2-NaCl solutions at the compositions, temperatures and pressures of our experiments. At these conditions, however, it is likely to be considerably lower than the solubility of quartz in pure water because the addition of NaCl or carbon dioxide, or both, will lower the activity of water and thus result in a decreased silica solubility. The decreased quartz solubility is also evidenced by the fact that the fluid in capsules loaded with a quartz core and an H_2O-CO_2-NaCl solution and run at high temperatures (600°C–800°C) and pressures (600 or 400 MPa) showed much less clouding from colloidal silica formation after the run, compared to pure water + quartz samples run at the same conditions. Furthermore, the effect of silicic acid on the volumetric properties of water is small and has an insignificant effect on solvus and isochore positions (Bodnar and Sterner, 1985; Sterner and Bodnar, 1991; Schmidt et al., 1998).

Because the presence of volatiles in solution can have a large effect on solvus positions, accurate control of the CO_2 concentration was essential in this study. Silver oxalate was used as the carbon dioxide source, which offers the advantage of accurate control of the composition over a large range of H_2O/CO_2 ratios. However, the enhanced silver solubility in chloride solutions at elevated P-T conditions had previously caused concerns about the applicability of silver oxalate in synthetic fluid inclusion studies (Plyasunova and Shmulovich, 1991). More recently, Krüger and Diamond (in press) conducted synthetic fluid inclusion experiments using silver oxalate as the carbon dioxide source. They showed that, indeed, silver does not act as an inert component in the system H_2O-NaCl-CO_2 at elevated temperatures. During capsule loading, silver oxalate reacts with the NaCl brine to form AgCl and $Na_2C_2O_4$. However, the subsequent dissolution of AgCl at higher temperatures to form an aqueous chloride solution was incomplete in their experiments. For the studied composition H_2O + 6 wt.% NaCl + 9.86 mol.% CO_2 (relative to water), they found HCO_3^-(aq) and chlorargyrite (AgCl) daughter crystals in all experiments and nahcolite in a few inclusions. In addition, a significant negative correlation between Th(L-V) and Tm(CLA) was observed. Furthermore, their calculated bulk molar volumes, based on measured Th(CO_2), were higher than molar volumes reported by Gehrig (1980) for Ag-free experiments at the same PTX conditions. Krüger and Diamond (in press) attributed the difference to the presence of HCO_3^- in the aqueous phase, which was not accounted for in the calculations. The "loss" of CO_2 to HCO_3^-(aq) lowered the density of the CO_2-rich vapor and, thus, resulted in lower Th(CO_2) values during homogenization to the vapor phase. However, average Th(L-V) were in good agreement (within ±10°C) with the results of Gehrig (1980).

The results of our study agree well with the observations of Krüger and Diamond (in press). In our study, nahcolite was observed in a number of experiments containing 20 or 40 wt.% NaCl relative to water. Due to the sluggish nature of nahcolite nucleation, this phase was initially only observed in a few high salinity inclusions but was found in many more samples when re-examined after 2 years. Likewise, bulk molar volumes calculated from the measured Th(CO_2) and the known bulk composition were usually about 2 cm^3/mol higher than molar volumes reported by Gehrig (1980) for the same PTX conditions. Molar volumes are not reported for our experiments because no data were available to correct for the amount of HCO_3^- in the aqueous solution.

In contrast to the study of Krüger and Diamond (in press), we did not find chlorargyrite (AgCl) in the inclusions synthesized in cold-seal pressure vessels using water as the pressure medium. Furthermore, we did not observe a significant correlation between Th(L-V) and Tm(CLA) or Th(CO_2) and Tm(CLA) for inclusions from such experiments. Chlorargyrite occurred only if argon was used as the pressure medium (during the IHPV experiments). The apparent absence of chlorargyrite in the "water-medium" runs is probably related to the fact that the hydrogen fugacity during these runs was different from that during the experiments of Krüger and Diamond (in press) where the pressure medium was argon. The presence of nahcolite in inclusions synthesized in our experiments implies that the excess chlorine in solution must be balanced by some species other than Na^+. We do not know which chlorine species are present. AgCl, which is very insoluble at room temperature, was not observed.

The salinity of inclusions formed in the one-phase field and containing ≤20 wt.% NaCl relative to water was repeatedly monitored using the dissociation temperatures of the CO_2 hydrate [Tm(CLA)] and generally deviated by at most ±1 wt.% from the expected value. Therefore, water loss during capsule welding was insignificant. Although our Tm(CLA) data show some scatter (usually ±0.3 to ±0.6°C), the average clathrate melting temperatures in the presence of aqueous brine, liquid CO_2, and CO_2-rich vapor for inclusions containing 6 and 20 wt.% NaCl are in good agreement with the experimental results for the "pure" H_2O-NaCl-CO_2 system reported by Chen (1972), and also with the study conducted by Diamond (1992), where silver oxalate was used for synthesis of H_2O-NaCl-CO_2 inclusions. Furthermore, halite dissolution temperatures for H_2O + 10 mol.% CO_2 + 40 wt.% NaCl inclusions (a number of inclusions in these samples contained small nahcolite crystals) measured in this study are about 20 degrees higher than the vapor-saturated halite liquidus of an aqueous solution containing 40 wt.% NaCl (Bodnar, 1994). Assuming that the shift in halite dissolution temperature is not related to the presence of carbon dioxide and is due exclusively to HCO_3^-(aq) in solution, the maximum compositional error would be about 1.7 wt.% NaCl relative to water, using the equation of Sterner et al. (1988). This indicates that the effect of HCO_3^-(aq) on the salinity determinations is not negligible, but is tolerable to achieve the goals of our study. We estimate that the overall uncertainties in the H_2O/NaCl and H_2O/CO_2 ratios are within ±0.5 to ±1 wt.% NaCl and about ±0.5 mol.% CO_2 of the values listed in Tables 1 and 4.

Homogenization temperatures of some samples show a slightly larger scatter than would be expected based on the uncertainty of the microthermometric measurements. However, the scatter in our Th(L-V) data is usually about ±5 to ±10°C (Table 1). This is in agreement with standard deviations of homogenization temperatures for Ag-free synthetic H_2O-NaCl-CO_2 inclusions reported by Frantz et al. (1992) which range from 1.7 to 14.2°C.

Iso-Th line slopes and solvus pressures obtained in this study for a bulk composition of H_2O + 10 mol.% CO_2 + 6 wt.% NaCl are in quite good agreement with data reported by Gehrig (1980) for essentially the same composition in the absence of silver. For this composition, the deviations between isochore slopes obtained by Gehrig (1980) and iso-Th line slopes determined in this study are comparable to the deviations between the data of Gehrig (1980) and the synthetic fluid inclusion data of Bodnar and Vityk (1994) for the binary compositions H_2O + 6 wt.% NaCl and H_2O + 20 wt.% NaCl. This agreement suggests that uncertainties in Th(L-V) related to the presence of silver do not contribute significantly to the overall experimental error within that (relatively small) compositional range. Differences between datasets for a bulk composition of H_2O + 10 mol.% CO_2 + 6 wt.% NaCl become larger as the homogenization temperature decreases. Errors in determination of dP/dT slopes of iso-Th lines are larger at lower solvus temperatures, where the homogenization temperature becomes increasingly independent from the formation temperature. Consequently, the calculated solvus pressure has larger uncertainty at lower Th(L-V) because it is obtained by extrapolating the iso-Th line to the corresponding homogenization temperature. In Table 3, we have indicated the Th(L-V) at which errors in the calculated slopes become too large to be useful for calculating solvus pressures.

Krüger and Diamond (in press) showed that Th(L-V) of inclusions prepared using silver oxalate were in good agreement with those synthesized using a gas loading apparatus (Frantz et al., 1989). This indicates that Th(L-V) from inclusions which use silver oxalate as the CO_2 source can be used to determine iso-Th lines and to estimate solvus pressures with acceptable accuracy. Prerequisites are a strong correlation of Tf with Th(L-V) and synthesis of the fluid inclusions at experimental conditions where the effect of compositional errors on Th(L-V) due to the reaction of silver oxalate with the fluid are relatively small. However, the validity of the latter prerequisite has so far only been evaluated for a relatively small range in composition. The good agreement between the results of our study and the datum obtained by Frantz et al. (1992) for the Ag-free system for the P-T shift of critical points as a function of composition can be taken as a further indication that the effect of $NaHCO_3$(aq) on the P-T location of the solvus is not large within the compositional range of this study.

2.4.2. Pressure–Temperature errors

The uncertainty in experimental pressure and temperature of cold-seal pressure vessels used here is about ±1% (Sterner and Bodnar, 1991). The pressure in the cold-seal bombs was measured using a Bourdon tube-type Heise gauge and a manganin cell. The calibration of both was checked against a factory calibrated transducer, which was also used to monitor the pressure in the IHPV. Up to 490 MPa, differences in pressure readings between these three devices were less than 3 MPa. To evaluate the error in experimental temperature due to thermal gradients within the bombs, platinum capsules (length 2.0–2.5 cm) containing pure water and a fractured quartz core were placed behind the H_2O-CO_2-NaCl capsules (that is, towards the "cold" end of the cold-seal pressure vessel) and run along with the water-carbon dioxide-salt samples. The average length of the H_2O-CO_2-NaCl capsules was about 3 cm. The homogenization temperatures of the pure H_2O synthetic inclusions formed during these runs were then used to

Table 1. Liquid-vapor homogenization temperatures and experimental conditions for synthetic fluid inclusions in the H_2O-NaCl-CO_2 system.

Sample number	Tf	Pf	Salinity	Mol.% CO_2	Th(L-V) (average)	Th(L-V) (range)	n	Method
012196-3	400	200	6	10	295 (L)	290–300	33	GHFS
012196-4	500	200	6	10	333 (L)	330–338	32	GHFS
012196-8	600	200	6	10	363 (L)	358–367	41	GHFS
031196-9	650	200	6	10	379 (L)	374–383	35	GHFS
031196-10	675	200	6	10	385 (C)	381–389	43	GHFS
021896-4	700	200	6	10	395 (V)	392–398	25	GHFS
012196-1	400	300	6	10	280 (L)	274–284	43	GHFS
012196-2	500	300	6	10	303 (L)	297–311	32	GHFS
012196-9	600	300	6	10	327 (L)	323–330	25	GHFS
021896-8	700	300	6	10	350 (L)	346–353	42	GHFS
050396-5	800	300	6	10	372 (L)	365–379	52	GHFS
021896-3	400	400	6	10	272 (L)	263–277	36	GHFS
021896-7	500	400	6	10	284 (L)	280–289	38	GHFS
031196-3	600	400	6	10	301 (L)	297–306	31	GHFS
021896-1	700	400	6	10	321 (L)	317–325	33	GHFS
031196-4	700	400	6	10	317 (L)	311–319	34	GHFS
012196-5	400	200	6	20	329 (L)	315–334	33	GHFS
012196-6	450	200	6	20	327 (L)	323–337	21	GHFS
012196-7	500	200	6	20	356 (V)	354–361	14	GHFS
040496-1	550	200	6	20	381 (V)	374–388	19	GHFS
021896-5	600	200	6	20	408 (V)	401–416	23	GHFS
040496-2	650	200	6	20	452 (V)	440–467	21	GHFS
031196-1	700	200	6	20	498 (V)	486–509	8	GHFS
021896-9	400	300	6	20	319 (L)	315–322	25	GHFS
021896-10	500	300	6	19.8	327 (L)	322–335	32	GHFS
021896-11	500	300	6	20	330 (L)	326–336	32	GHFS
031196-5	600	300	6	20	347 (L)	344–354	26	GHFS
					350 (C)	346–355	8	GHFS
					351 (V)	346–357	7	GHFS
040496-3	700	300	6	20	370 (V)	367–377	25	GHFS
050396-4	800	300	6	20	417 (V)	408–425	25	GHFS
011895-9	300	200	20	9.9		Immiscible fluid		
011895-3	350	200	20	10		Immiscible fluid		
011895-4	400	200	20	10	376 (L)	374–378	9	GHFS
031295-5	450	200	20	10	400 (L)	391–407	24	GHFS
011895-6	500	200	20	10	415 (L)	411–418	13	GHFS
041395-11	550	200	20	10	458 (L)	450–466	44	GHFS
011895-1	600	200	20	10	494 (L)	487–497	16	GHFS
020295-4	650	200	20	10	533 (L)	525–543	32	GHFS
011895-2	700	200	20	10	594 (V,C)	588–600	5	GHFS
041395-10	400	300	20	10	362 (L)	456–365	17	GHFS
042395-9	450	300	20	10	379 (L)	374–383	21	GHFS
042395-7	500	300	20	10	394 (L)	390–398	23	GHFS
062895-4	500	300	20	10	393 (L)	386–397	34	GHFS
042395-1	550	300	20	10	408 (L)	401–412	39	GHF
041395-6	600	300	20	10	433 (L)	426–436	27	GHFS
062895-3	600	300	20	10	433 (L)	428–444	36	GHFS
042395-3	650	300	20	10	453 (L)	446–460	20	GHFS
062895-2	650	300	20	10	444 (L)	431–459	39	GHFS
062895-1	700	300	20	9.9	467 (L)	457–480	35	GHFS
050396-3	800	300	20	9.9	498 (L,C)	495–501	13	GHFS
					538 (L,C)	536–540	9	GHFS
011895-7	300	400	20	10		Immiscible fluid		
031295-1	400	400	20	10	353 (L)	346–358	13	GHFS
031295-4	450	400	20	10	363 (L)	360–366	22	GHFS
011895-8	500	400	20	10	378 (L)	376–381	15	GHFS
041395-7	550	400	20	10	385 (L)	383–388	40	GHFS
031295-2	600	400	20	10	405 (L)	402–414	36	GHFS
031295-3	650	400	20	10	418 (L)	413–421	42	GHFS
020295-5	700	400	20	10	427 (L)	418–432	24	GHFS
042395-8	450	500	20	10	356 (L)	353–357	8	GHFS
042395-5	500	500	20	10	360 (L)	358–362	34	GHFS
042395-4	550	500	20	9.9	368 (L)	365–373	33	GHFS
042395-6	600	500	20	10	378 (L)	374–382	25	GHFS
062895-5	650	500	20	10	388 (L)	382–402	53	GHFS

(Continued)

Table 1. (Continued)

Sample number	Tf	Pf	Salinity	Mol.% CO_2	Th(L-V) (average)	Th(L-V) (range)	n	Method
062895-6	700	500	20	10	402 (L)	394–411	30	GHFS
020295-8	400	200	20	20		Immiscible fluid		
022695-1	450	200	20	20.1		Immiscible fluid		
020295-7	500	200	20	20.1		Immiscible fluid		
022695-4	600	200	20	20		Immiscible fluid		
022695-3	650	200	20	19.9		Immiscible fluid		
022695-2	700	200	20	20.1		Immiscible fluid		
032595-3	400	300	20	20		Immiscible fluid		
051595-4	450	300	20	20		Immiscible fluid		
051595-3	500	300	20	20	473 (L)	466–481	10	GHFS
					479 (L)	477–481	2	HDAC
071195-4	550	300	20	19.9	516 (L)	514–518	9	GHFS
032595-2	600	300	20	20	577 (V)	574–582	4	GHFS
					545 (C,V)	539–551	3	HDAC
060695-6	650	300	20	20	591 (V)	589–595	5	GHFS
032595-4	700	300	20	20	631 (V)	622–639	13	GHFS
					608 (V)	598–618	2	HDAC
060695-2	400	400	20	20		Immiscible fluid		
060695-1	450	400	20	20		Immiscible fluid		
060695-3	500	400	20	20	462 (L)	460–464	3	HDAC
031295-6	700	400	20	20	556? (V)		1	GHFS
					540 (C,L)	530–550	2	HDAC
071195-1	400	500	20	20		Immiscible fluid		
071195-2	450	500	20	19.9		Immiscible fluid		
060695-5	500	500	20	20	455 (L)	452–458	2	HDAC
051595-2	600	500	20	20.1	480 (L)	476–484	6	HDAC
102093-14	400	200	40	5	395 (L)[a]	391–398[a]	7	GHFS
041894-4	450	200	40	5	434 (L)[a]		1	GHFS
041894-10	450	200	40	5	432 (L)[a]	423–441[a]	5	GHFS
102093-13	500	200	40	5	472 (L)[a]	467–476[a]	8	GHFS
102093-10	550	200	40	5	509 (L)[a]	506–511[a]	12	GHFS
041894-6	625	200	40	5	583 (L)[a]	579–586[a]	10	GHFS
041894-5	650	200	40	5	597 (L)[a]	592–601[a]	7	GHFS
041894-7	700	200	40	5	625 (L)[a]	617–630[a]	7	GHFS
091295-2	400	300	40	5	379 (L)	377–382	5	GHFS
091295-5	500	300	40	5	435 (L)	432–437	14	GHFS
091295-7	600	300	40	5	481 (L)	475–486	25	GHFS
032396-2	700	300	40	5	526 (L)	518–534	24	GHFS
042796-5	800	300	40	5	579 (L)	572–587	2	GHFS
070793-8	350	400	40	5	343? (L)	341–345[a]	2	GHFS
041894-8	400	400	40	5	372 (L)[a]	363–378[a]	8	GHFS
070793-5	450	400	40.1	4.9	392 (L)[a]	388–393[a]	10	GHFS
081293-8	500	400	40	5	411 (L)[a]	408–413[a]	11	GHFS
102093-7	550	400	40	5	428 (L)[a]	425–432[a]	11	GHFS
102093-6	600	400	40	5	450 (L)[a]	446–452[a]	20	GHFS
102093-9	650	400	40	5	476 (L)[a]	474–477[a]	12	GHFS
041894-9	650	400	40.1	5	472 (L)[a]	470–473[a]	12	GHFS
081293-6	700	400	40	5	484 (L)[a]	479–489[a]	14	GHFS
032396-4	400	300	40	10		Immiscible fluid		
091295-4	500	300	40	10	491 (L)	479–500	14	GHFS
					490 (L)	485–495	2	HDAC
032396-6	600	300	40	10	592 (L)	588–596	16	GHFS
					579 (L)	574–584	4	HDAC
032396-10	700	300	40	10	633 (L)	625–639	9	GHFS
					659 (L)	654–663	7	GHFS
					656 (L)	651–661	3	HDAC
032396-7	400	400	40	10		Immiscible fluid		
032396-8	500	400	40	10	488 (L)	481–495	5	HDAC
042796-4	600	400	40	10	575 (L)	571–578	3	GHFS
					556 (L)	546–566	5	HDAC
042796-1	700	400	40	10	615 (L)	608–625	5	GHFS
					586 (L)	581–591	2	HDAC

(Continued)

Table 1. (Continued)

Sample number	Tf	Pf	Salinity	Mol.% CO_2	Th(L-V) (average)	Th(L-V) (range)	n	Method
032396-3	400	500	40	10		Immiscible fluid		
042796-2	500	500	40	10	488 (L)	486–490	7	HDAC
042796-6	600	500	40	10	515 (L)	508–522	4	HDAC
042796-3	700	500	40	10	559 (L)	549–569	7	HDAC

Homogenization temperatures are only reported for samples which formed in the one-phase field. Tf = formation temperature (°C); Pf = formation pressure (MPa); Salinity = NaCl concentration of the solution in weight percent relative to H_2O; Mol.% CO_2 = carbon dioxide concentration in mol percent relative to H_2O; Th(L-V) (average) = average liquid-vapor homogenization temperature (°C); Th(L-V) (range) = the range in measured Th(L-V) (°C); (L) = homogenization to the liquid, aqueous phase; (V) = homogenization to the vapor, CO_2-rich phase; (C) = homogenization by critical behavior; *n* = number of measured inclusions; GHFS = gas-flow heating/freezing stage; HDAC = hydrothermal diamond-anvil cell (data from Schmidt et al., 1998).

[a] Data from Schmidt et al. (1995).

calculate isochores based on the specific volumes of water given by Haar et al. (1984), which were corrected for thermal expansion of quartz using the equation of Hosieni et al. (1985). The formation temperature of the pure water inclusions was then calculated by intersecting these isochores with the corresponding experimental pressures. These calculated formation temperatures were within 10°C of the thermocouple temperatures. Thus, the uncertainty in formation temperature of inclusions synthesized in cold-seal vessels is less than ±10°C. The uncertainty in experimental temperature in the IHPV is about ±10° at 800°C; the pressure error is approximately ±1%. The thermal gradient across the platinum capsule length of about 4 cm was estimated to be 5°C (J. Student, personal communication).

A lower effective pressure for the fluid in the fractures compared to the externally applied pressure can result if the amount of fluid in the capsule is too small (Krüger and Diamond, in press). However, calculation of the degree of capsule filling requires knowledge of the molar volume of the fluid at the experimental P and T. In our experiments, the molar volume is only known at a few PTX conditions. Generally, we used a similar capsule size, but larger quartz rods and more fluid than Krüger and Diamond (in press), so the degree of fill was probably sufficient in most of our experiments to ensure equality of applied and effective pressure. The degree of filling may have been too low in a few runs in the high-pressure low-temperature region (e.g., run number 021896-3).

Microthermometric measurements in the gas-flow stage have the following estimated accuracy: ±0.5°C at about −50° to −60°C, approximately ±0.2°C between −10°C and +30°C, and better than ±2°C for temperature measurements up to 400°C. Above that temperature, the accuracy decreases to about ±5°C at 600°C. Temperatures determined using a hydrothermal diamond–anvil cell have a similar or perhaps somewhat lower uncertainty (c.f., Shen et al., 1993).

3. RESULTS AND DISCUSSION

3.1. Liquid-Vapor Curves and Iso-Th Lines

Iso-Th lines in the one-phase field and high pressure portions of the liquid-vapor curve (with one exception) were obtained for the following compositions:

1) $X(H_2O) = 0.7949$, $X(NaCl) = 0.1633$, $X(CO_2) = 0.0418$ (H_2O + 40 wt.% NaCl + 5 mol.% CO_2),
2) $X(H_2O) = 0.7595$, $X(NaCl) = 0.1561$, $X(CO_2) = 0.0844$ (H_2O + 40 wt.% NaCl + 10 mol.% CO_2),
3) $X(H_2O) = 0.8416$, $X(NaCl) = 0.0649$, $X(CO_2) = 0.0935$ (H_2O + 20 wt.% NaCl + 10 mol.% CO_2),
4) $X(H_2O) = 0.7535$, $X(NaCl) = 0.0581$, $X(CO_2) = 0.1884$ (H_2O + 20 wt.% NaCl + 20 mol.% CO_2),
5) $X(H_2O) = 0.8843$, $X(NaCl) = 0.0174$, $X(CO_2) = 0.0983$ (H_2O + 6 wt.% NaCl + 10 mol.% CO_2), and
6) $X(H_2O) = 0.7876$, $X(NaCl) = 0.0155$, $X(CO_2) = 0.1969$ (H_2O + 6 wt.% NaCl + 20 mol.% CO_2).

The solvus for H_2O + 6 wt.% NaCl + 20 mol.% CO_2 was interpolated from the data published by Gehrig (1980), which was more accurate than the solvus based on the few samples of this composition synthesized in this study. For the compositions H_2O + 40 wt.% NaCl + 10 mol.% CO_2 and H_2O + 20 wt.% NaCl + 20 mol.% CO_2, the liquid-vapor curve locations are based on petrographic and microthermometric evidence for the absence of unmixing. The iso-Th lines were calculated from Th(L-V) data normalized to the solvus pressure, because these homogenization temperatures were determined at different confining pressures using a hydrothermal diamond–anvil cell (Table 1). All other iso-Th lines and solvi are based on homogenization temperatures measured at one atmosphere confining pressure using a gas-flow stage (Table 1). Table 2 lists regression equations of formation temperature [Tf] as a function of homogenization temperature [Th] along isobars of formation pressure. All iso-Th line slopes derived from homogenization temperature data, and liquid-vapor curves that were located using the "slope-intercept" technique (i.e., the solvi of the compositions H_2O + 6 wt.% NaCl + 10 mol.% CO_2, H_2O + 20 wt.% NaCl + 10 mol.% CO_2, and H_2O + 40 wt.% NaCl + 5 mol.% CO_2), were calculated from these equations. Smoothed iso-Th line slopes and solvus pressures in the PTX range of this study are given in Table 3.

The slopes of iso-Th lines at a constant homogenization temperature increase along pseudobinaries with the addition of carbon dioxide and particularly with the addition of NaCl (Table 3), which partly reflects collapse of the water structure. For compositions ≤20 mol.% CO_2 and a constant salinity, the high-pressure portion of the solvus shifts to significantly higher pressures and temperatures as the carbon dioxide concentration increases. The same effect was observed for a constant H_2O/CO_2 ratio with addition of NaCl (Fig. 3). In the pseudobinary (H_2O + 20 wt.% NaCl)-CO_2, the solvus expands rapidly towards very high pressures and temperatures as the CO_2 concentration exceeds 20 mol.%. Samples having compositions of H_2O + 20 wt.% NaCl + 30 to 70 mol.% CO_2 showed clear evidence of unmixing at all P-T conditions up to 700°C and 500 MPa, with the possible exception of a 30 mol.% CO_2 run at 500 MPa formation pressure and 700°C formation temperature.

Table 2. Regression coefficients (A, B, C) of empirical equations [$Tf = A \cdot (Th)^2 + B \cdot Th + C$] relating homogenization temperature (Th) and formation temperature (Tf) of synthetic fluid inclusions in the H_2O-NaCl-CO_2 system along isobars of formation pressure (Pf).

Wt.% NaCl	Mol.% CO_2	Pf	A	B	C	Valid Th range (°C)
6	10	200	0	3.0598	−508.93	300–400
6	10	300	0	4.3281	−812.7	275–400
6	10	400	0	6.1721	−1265.47	275–325
6	20	200	−0.004652585	5.3592	−816.74	(330) 350–500
6	20	300	−0.02452468	21.7081	−3986.1	330–415
20	10	200	−0.003440963	4.6804	−867.45	370–600
20	10	300	−0.006702883	8.4541	−1789.24	360–400 (500)
			0	2.4592	−466.07	390–600
20	10	400	0	3.8645	−956.6	360–450
20	10	500	0	5.2552	−1397.45	360–400
20	20	300	0	1.5501	−243.26	475–600
20	20	400	0	2.5478	−675.8	475–600
20	20	500	0	4	−1320	460–500
40	5	200	0	1.2504	−91.91	390–625
40	5	300	0	2.0336	−376.14	375–575 (625)
40	5	400	0	2.5411	−544.46	375–500
40	10	300	0	1.2027	−91.57	500–650
40	10	400	0	1.9434	−455.92	500–600 (650)
40	10	500	0	2.7641	−839.16	500–575

Th = homogenization temperature (°C); Tf = formation temperature (°C); Pf = formation pressure (MPa); Wt.% NaCl = NaCl concentration of the solution in weight percent relative to H_2O; Mol.% CO_2 = carbon dioxide concentration in mol percent relative to H_2O; numbers in parentheses = Th range probably applicable to this value, but with a higher uncertainty in the resulting iso-Th line slope.

Table 3. Slopes of iso-Th lines in the one-phase field and solvus pressures as functions of homogenization temperature and composition for parts of the high-pressure portion of the liquid-vapor curve in the system H_2O-NaCl-CO_2.

Wt.% NaCl	Mol.% CO_2	Th (°C)	Slope (MPa/°C)	Ph (MPa)	Wt.% NaCl	Mol.% CO_2	Th (°C)	Slope (MPa/°C)	Ph (MPa)
6	10	275	1.84[a]	111	20	20	525	1.03	250[b]
6	10	300	1.11	88	20	20	540 = Tc	0.93	250 = Pc[b]
6	10	325	0.81	69	20	20	550	0.86	250[b]
6	10	350	0.68	56	20	20	575	0.71	250[b]
6	10	375	0.59	47	20	20	600	0.61	250[b]
6	10	385 = Tc	0.55	45 = Pc	40	5	375	4.55[a]	250
6	10	400	0.49	44	40	5	400	3.15[a]	178
6	20	330	1.62[a]	(196.5)	40	5	425	2.2	169
6	20	350 = Tc	0.845	82.5 (141.5) = Pc	40	5	450	1.58	165
6	20	375	0.6	102 (105.5)	40	5	475	1.2	163.5
6	20	400	0.525	104 (90)	40	5	500	0.96	164
6	20	415	0.51	101 (85)	40	5	525	0.82	165
20	10	360	1.86	247	40	5	550	0.71	166.5
20	10	380	1.57	177	40	5	575	0.62	168
20	10	400	1.32	138	40	5	600	0.54	169
20	10	425	1.08	118	40	5	625	0.48	170
20	10	450	0.9	117	40	10	488		370[b]
20	10	475	0.75	124	40	10	490		280[b]
20	10	500	0.64	132	40	10	500	4.05	260[b]
20	10	550 = Tc	0.47	148 = Pc	40	10	525	2.96	250[b]
20	10	600	0.32	164	40	10	550	2.19	250[b]
20	20	455		350[b]	40	10	575	1.64	250[b]
20	20	462		300[b]	40	10	600	1.24	250[b]
20	20	475	2.3[a]	260[b]	40	10	625	0.96	250[b]
20	20	500	1.34	250[b]	40	10	650	0.74	250[b]

Unless marked, reported slopes and solvus pressures were calculated based on the equations given in Table 2 and smoothed. For the composition H_2O + 6 wt.% NaCl + 20 mol.% CO_2, the more accurate solvus pressures interpolated from data published by Gehrig (1980) are given in parentheses. Wt.% NaCl = NaCl concentration of the solution in weight percent relative to H_2O; Mol.% CO_2 = carbon dioxide concentration in mol percent relative to H_2O; Th = homogenization temperature; Tc = critical temperature; slope = calculated slope of iso-Th lines in the one-phase field; Ph = homogenization pressure (= solvus pressure); Pc = critical pressure.

[a] = slopes are probably too high.

[b] = Ph estimated based on petrographic and microthermometric evidence for immiscibility and homogenization temperature data.

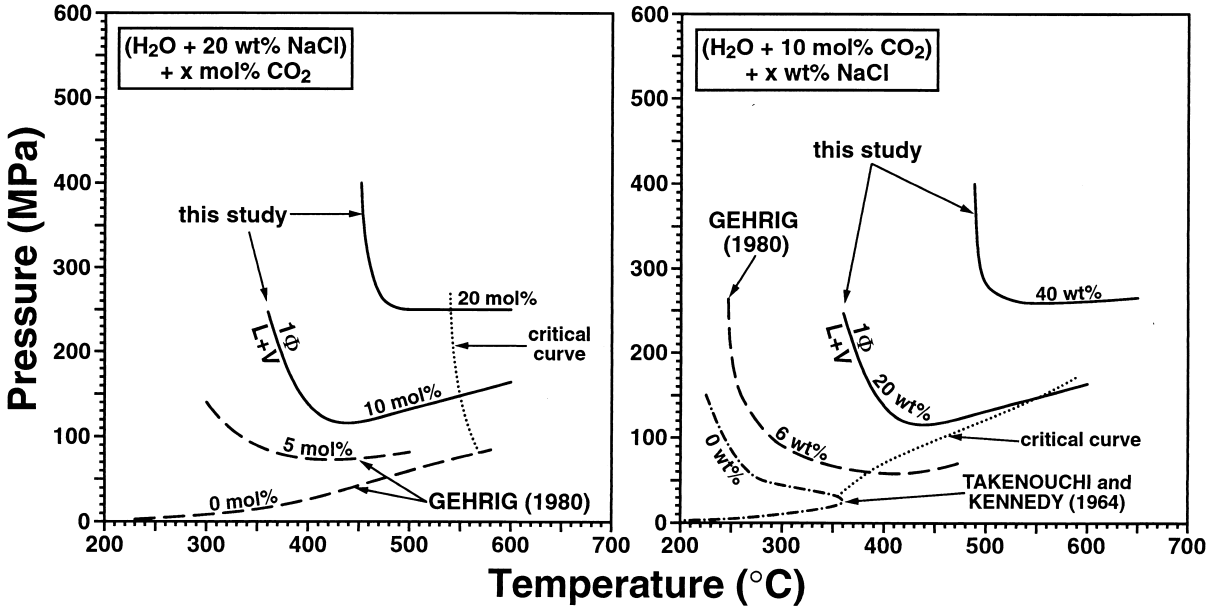

Fig. 3. Critical curves and high-pressure portions of solvi of the pseudobinaries (H_2O + 20 wt.% NaCl)-CO_2 and (H_2O + 10 mol.% CO_2)-NaCl. 1Φ = one-phase field; L + V = coexisting liquid and vapor.

This confirms the conclusion of Johnson (1991) that immiscibility is possible in this ternary system even at granulite-facies P-T conditions at salinities above 23 wt.% NaCl and intermediate mole fractions of carbon dioxide [$X(CO_2) > 0.3$].

3.2. Critical Properties

Physical and thermodynamic properties of aqueous solutions, such as heat capacity and viscosity, show extrema in the critical region in P-T space (Pitzer, 1986). Knowledge of critical properties in the system H_2O-NaCl-CO_2 is, therefore, of importance for numerical simulations of crustal fluid-flow and fluid-rock interaction (Bodnar and Costain, 1991) and supercritical water oxidation technology (Bodnar, 1995). In this study, critical temperatures and pressures were determined for four bulk compositions: H_2O + 6 wt.% NaCl + 10 mol.% CO_2, H_2O + 6 wt.% NaCl + 20 mol.% CO_2, H_2O + 20 wt.% NaCl + 10 mol.% CO_2, and H_2O + 20 wt.% NaCl + 20 mol.% CO_2 (the concentrations of NaCl and CO_2 are relative to water). The obtained data are plotted in Figure 4, along with experimental data from Tödheide and Franck (1963) and Knight and Bodnar (1989) for the binary subsystems and a single critical point for a ternary composition reported by Frantz et al. (1992). These data were used to construct a critical surface in P-T space that is plotted along pseudobinaries in Figure 4.

Addition of carbon dioxide in the experimentally studied compositional range results in a significant increase in the critical pressure and a slight lowering of critical temperatures. The main consequence of a rise in NaCl concentration is a large increase in critical temperature, whereas the critical pressure increases only moderately. Thus, the net effect of addition of both sodium chloride and carbon dioxide to water is generally

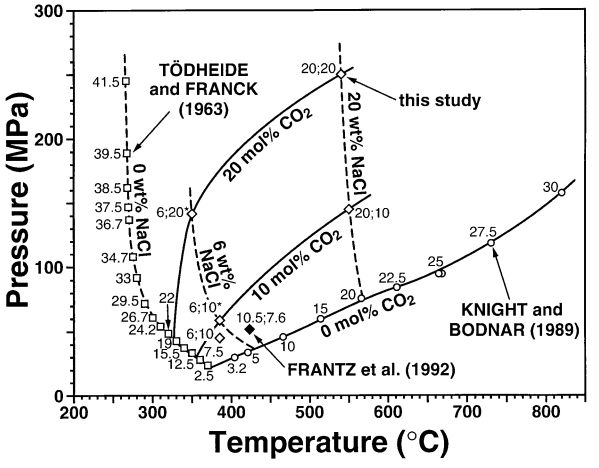

Fig. 4. P-T plot of the upper critical surface in the system water-sodium chloride-carbon dioxide along constant H_2O/NaCl ratios of 0, 6, and 20 wt.% NaCl (dashed lines) and constant H_2O/CO_2 ratios of 0, 10, and 20 mol.% CO_2 (solid lines). Data for the binary H_2O-CO_2 (squares) are from Tödheide and Franck (1963). The numbers close to the squares denote the carbon dioxide concentration in mol.%. Data for H_2O-NaCl (circles, labeled with the salinity in wt.% NaCl) are from Knight and Bodnar (1989). The critical points for ternary mixtures are based on the experimental data of Frantz et al. (1992) (solid diamond) and this study (open diamonds). The first number at the diamonds refers to the NaCl concentration in wt.% relative to H_2O, the second number gives the CO_2 concentration in mol.% relative to H_2O. An asterisk denotes that the critical pressure was calculated from solvus data obtained by Gehrig (1980).

Table 4. Halite dissolution temperatures in presence of liquid and vapor for synthetic fluid inclusions in the H_2O-NaCl-CO_2 system.

Sample number	Tf	Pf	Salinity	Mol.% CO_2	Tm(H + L + V → L + V) (average)	Tm(H + L + V → L + V) (range)	n	Method
102093-14	400	200	40	5	332.4[a]	330.0–333.6[a]	8	GHFS
041894-4	450	200	40	5	334.1[a]	333.0–336.7[a]	9	GHFS
041894-10	450	200	40	5	333.8[a]	331.5–335.6[a]	11	GHFS
102093-13	500	200	40	5	331.5[a]	330.0–334.4[a]	11	GHFS
102093-10	550	200	40	5	337.6[a]	336.9–338.3[a]	10	GHFS
041894-6	625	200	40	5	337.8[a]	337.1–338.7[a]	12	GHFS
041894-5	650	200	40	5	337.6[a]	334.4–341.5[a]	13	GHFS
041894-7	700	200	40	5	339.0[a]	337.0–340.3[a]	8	GHFS
091295-2	400	300	40	5	331.9	329.6–334.1	12	GHFS
091295-5	500	300	40	5	333.9	331.6–335.1	14	GHFS
091295-7	600	300	40	5	336.0	333.0–338.0	15	GHFS
032396-2	700	300	40	5	333.5	332.2–335.8	15	GHFS
042796-5	800	300	40	5	335.1	330.6–338.8	4	GHFS
070793-8	350	400	40	5	≈332[a]		1	GHFS
041894-8	400	400	40	5	333.7[a]	332.1–335.1[a]	6	GHFS
070793-5	450	400	40.1	4.9	334.7[a]	333.7–336.9[a]	11	GHFS
081293-8	500	400	40	5	334.5[a]	333.8–335.4[a]	11	GHFS
102093-7	550	400	40	5	334.0[a]	332.8–334.6[a]	11	GHFS
102093-6	600	400	40	5	335.9[a]	334.0–337.8[a]	20	GHFS
102093-9	650	400	40	5	341.4[a]	340.7–342.3[a]	12	GHFS
041894-9	650	400	40.1	5	336.6[a]	335.4–338.0[a]	11	GHFS
081293-6	700	400	40	5	336.4[a]	333.9–338.2[a]	14	GHFS
091295-4	500	300	40	10	345.4	341.6–348.1	22	GHFS
032396-6	600	300	40	10	340.9	337.6–344.4	20	GHFS
					342.5	338–347	8	HDAC
032396-10	700	300	40	10	339.5	336.5–344.3	27	GHFS
					342.5	341–343	3	HDAC
032396-8	500	400	40	10	344.2	340.8–346.1	20	GHFS
					344	343–345	4	HDAC
042796-4	600	400	40	10	341.6	340.1–343.2	20	GHFS
					341.5	341–342	2	HDAC
042796-1	700	400	40	10	340.8	336.2–343.3	10	GHFS
					341.5	340–343	4	HDAC
042796-2	500	500	40	10	340.3	338.7–342.6	15	GHFS
					341.5		1	HDAC
042796-6	600	500	40	10	339.4	337.0–341.0	16	GHFS
					340	339–341	4	HDAC
042796-3	700	500	40	10	342.7	334.7–346.7	19	GHFS
					339		1	HDAC

Tf = formation temperature (°C); Pf = formation pressure (MPa); Salinity = NaCl concentration of the solution in weight percent relative to H_2O; Mol.% CO_2 = carbon dioxide concentration in mol percent relative to H_2O; Tm(H + L + V → L + V) (average) = average halite dissolution temperature in presence of liquid and vapor (°C); Tm(H + L + V → L + V) (range) = the range in measured Tm(H + L + V → L + V) (°C); n = number of measured inclusions; GHFS = gas-flow heating/freezing stage; HDAC = hydrothermal diamond-anvil cell, data from Schmidt et al. (1998).

[a] Data from Schmidt et al. (1995); n.d. = not determined.

a large shift of the critical point towards both higher pressures and temperatures.

3.3. Halite Liquidi

Temperatures of halite dissolution in the presence of aqueous brine and CO_2-rich vapor [Tm halite] were determined for compositions containing 40 wt.% NaCl (Table 4). All measured inclusions in this pseudobinary had consistently higher halite dissolution temperatures compared to the H_2O-vapor-saturated halite liquidus temperature of 323°C for a 40 wt.% NaCl solution obtained by Bodnar (1994). A slight positive correlation between Tm halite and Th(L-V) was found for inclusions containing 5 mol.% CO_2 relative to water. The bubble-point curve may intersect the halite liquidus for this composition at a very high pressure outside the experimental pressure range of this study. If that point of intersection exists, it occurs at about 329°C. This temperature was calculated by linear regression of the total homogenization and halite dissolution temperature data and extrapolation of that line to Tm halite = Th(L-V). No relationship between Tm halite and Th(L-V) was found for a carbon dioxide concentration of 10 mol.%. At this composition, the temperature of the equilibrium halite + liquid + vapor = liquid + vapor averaged 342 ± 6°C and appeared to be essentially independent of pressure up to about 200 MPa (decrepitation occurred rarely at that temperature). There was generally very good agreement between halite dissolution temperatures determined using a gas-flow heating stage at 0.1 MPa confining pressure and those measured in a diamond-anvil cell at higher confining pressure (Schmidt et al., 1998). The in-

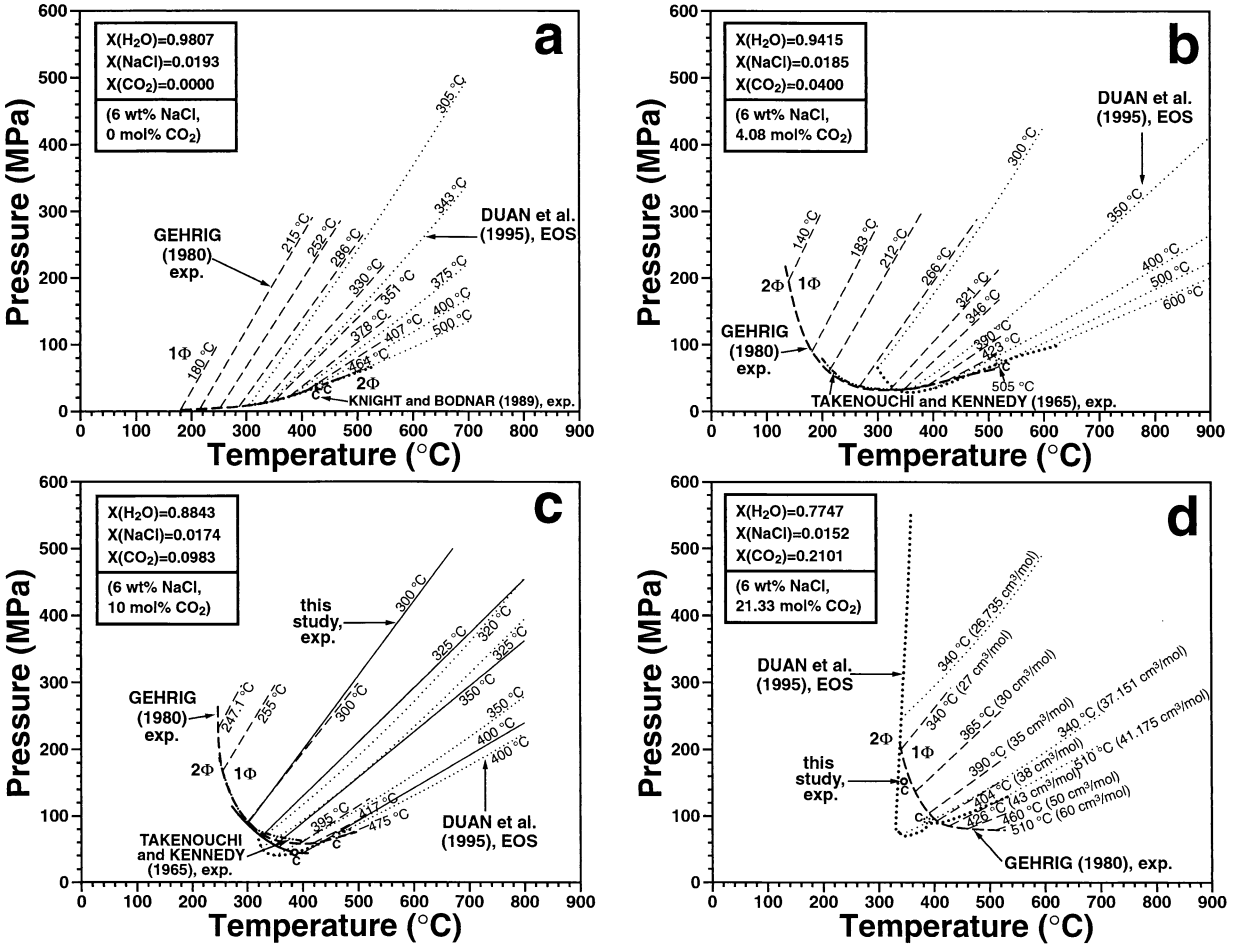

Fig. 5. High-pressure portions of the solvus, critical points, and lines of equal homogenization temperature for constant compositions along the pseudobinary (H_2O + 6 wt.% NaCl)-CO_2. Heavy lines refer to solvi; thin lines refer to lines of equal homogenization temperature in the one-phase field, labeled with the corresponding homogenization temperature. The experimental data are from this study (solid lines), Gehrig (1980) (dashed lines), Takenouchi and Kennedy (1965) (dot-dot-dashed lines), and Knight and Bodnar (1989) (square). The dotted lines were calculated using the equation of state of Duan et al. (1995). 1Φ = one-phase field; 2Φ = coexisting liquid and vapor; C = critical point.

crease in halite dissolution temperature with carbon dioxide concentration could be caused by the presence of $NaHCO_3$ in the aqueous phase, and/or water loss from the aqueous liquid phase to the carbonic vapor phase.

3.4. Comparison of experimental data with the equation of state of Duan et al. (1995)

Microthermometric data obtained from fluid inclusions represent one of the most important sources of P-T information for understanding the geologic history of rocks and minerals. In such cases, isochores and solvus pressures are usually inferred from homogenization temperatures and inclusion compositions. Here we present a number of isoplethic P-T phase diagrams of the system H_2O-NaCl-CO_2 for compositions along the pseudobinaries (H_2O + 6 wt.% NaCl)-CO_2 (Fig. 5), (H_2O + 20 wt.% NaCl)-CO_2 (Fig. 6), and (H_2O + 40 wt.% NaCl)-CO_2 (Fig. 7). These diagrams depict P-T locations of a high-pressure portion of the solvus, critical points, lines of constant homogenization temperature, and a portion of the halite liquidus for 40 wt.% NaCl compositions. The diagrams include empirical results from literature data, experimental results of this study, and phase equilibria and isochores calculated using the equation of state formulated by Duan et al. (1995). Duan et al. (1995) report that their equation of state "consistently predicts various properties including PVTX, immiscibility or phase equilibria, solubilities, and activities with an accuracy close to that of experimental data from 300 to about 1000°C and 0–6000 bar with NaCl concentrations to about 30 wt.% NaCl (relative to NaCl + H_2O) or to about 50 wt.% with less accuracy." The isochores and phase equilibria calculated from that equation of state for compositions containing 40 wt.% NaCl (Fig. 7) should therefore be considered as a first approximation and used only with caution for a comparison to the experimental data. The empirical data presented were obtained using a variety of experimental techniques, including:

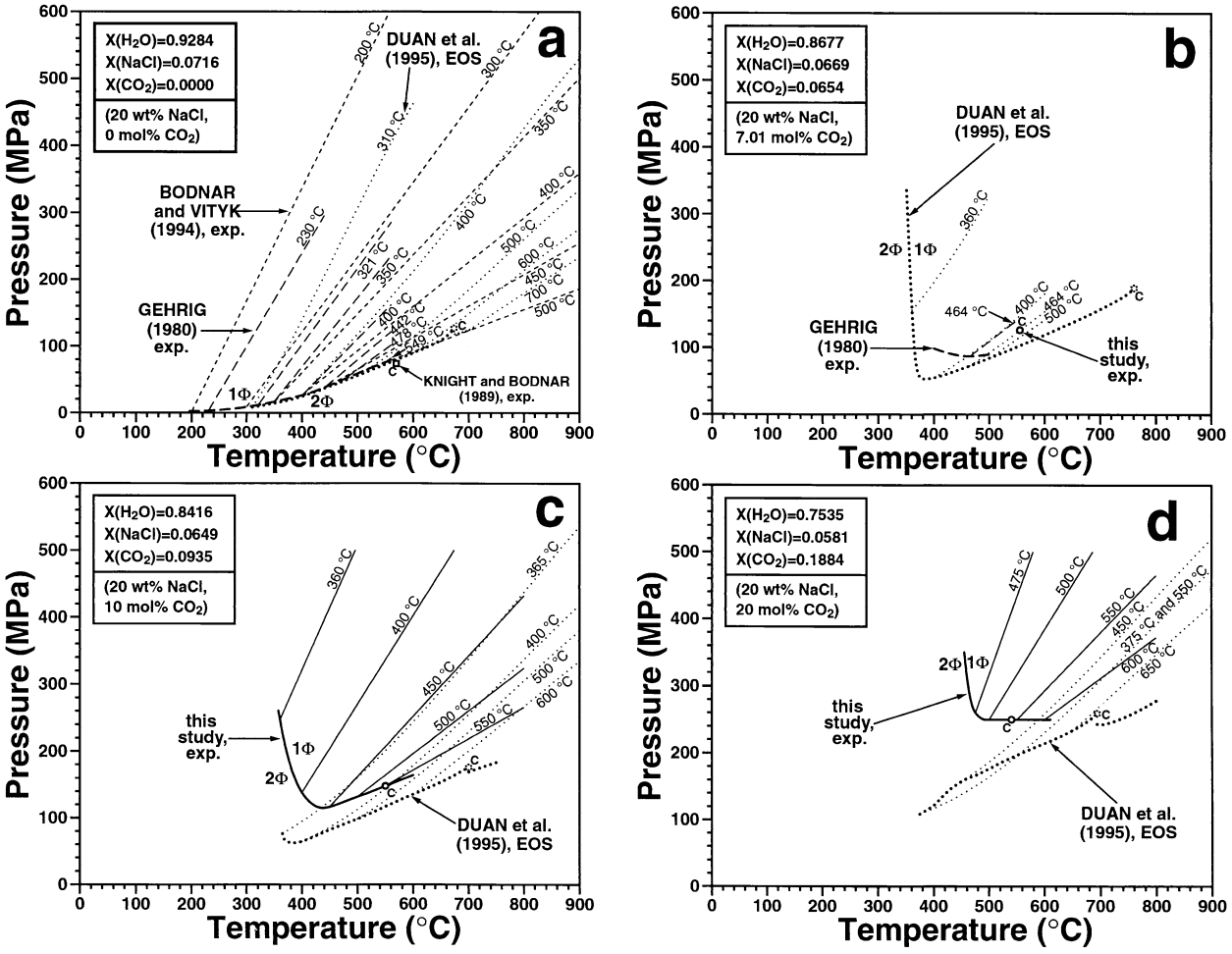

Fig. 6. High-pressure portions of the solvus, critical points, and lines of equal homogenization temperature for constant compositions along the pseudobinary (H_2O + 20 wt.% NaCl)-CO_2. Heavy lines refer to solvi; thin lines refer to lines of equal homogenization temperature in the one-phase field, labeled with the corresponding homogenization temperature. The experimental data are from this study (solid lines), Gehrig (1980) (long dashed lines), Bodnar and Vityk (1994) (short dashed lines), and Knight and Bodnar (1989) (square). The dotted lines were calculated using the equation of state of Duan et al. (1995). 1Φ = one-phase field; 2Φ = coexisting liquid and vapor; C = critical point.

- A large, variable-volume autoclave equipped with a sapphire window (Gehrig, 1980);
- An autoclave equipped with a device to sample liquid and vapor phases separately (Takenouchi and Kennedy, 1965);
- Synthetic fluid inclusions, CO_2 (and Ag) free compositions (Knight and Bodnar, 1989; Bodnar and Vityk, 1994; Bodnar, 1994; Schmidt et al., 1998); and
- Synthetic fluid inclusions, use of silver oxalate as carbon dioxide source (Schmidt et al., 1995, 1998; this study).

The data from these various experimental studies are usually in good agreement. The solvus pressures obtained in this study, which were calculated by extrapolation of iso-Th lines or by bracketing between formation pressures, can show relatively large deviations from the data of Gehrig (1980) at some experimental conditions. Many solvus data of Gehrig (1980) were obtained by direct observation and should be considered as more accurate.

With the exception of some critical point locations, there is good agreement between the equation of state and the experimental data at $X(CO_2) = 0$ where the equation of Duan et al. (1995) is identical to the equation of Anderko and Pitzer (1993). Although the equation of state of Duan et al. (1995) seems to reproduce the molar volumes obtained by Gehrig (1980) well (their Table 6 and Fig. 8, not shown here), significant deviations can occur between calculated and experimentally obtained P-T locations of solvi and isochores with increasing $X(CO_2)$, particularly at homogenization temperatures of less than about 400°C (Figs. 5 and 6). The largest disagreements between results predicted by the equation of state formulated by Duan et al. (1995) and the experimental data occur at compositions outside the compositional range of the experimental data used to develop the equation of state. The agreement between the P-T locations of experimentally determined and modeled solvi and iso-Th lines tends to improve with

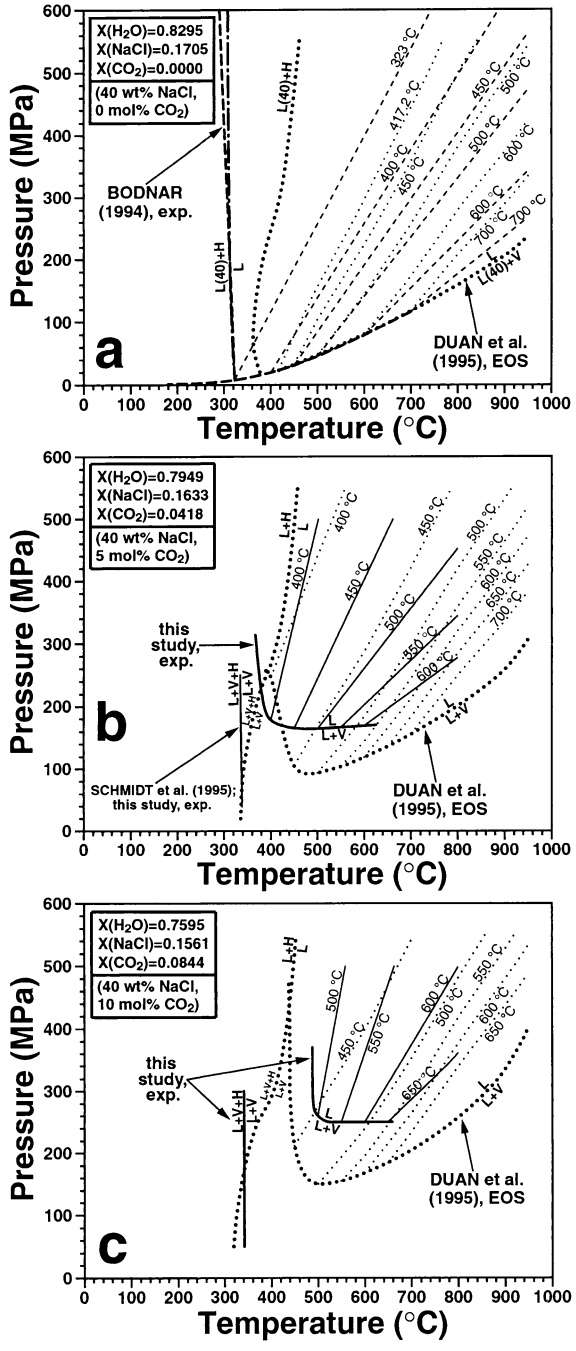

Fig. 7. Liquidi, high-pressure portions of the solvus, and lines of equal homogenization temperature for constant compositions along the pseudobinary (H_2O + 40 wt.% NaCl)-CO_2. Heavy lines refer to phase equilibria; thin lines refer to lines of equal homogenization temperature in the one-phase field, labeled with the corresponding homogenization temperature. The experimental data are from this study (solid lines), Bodnar (1994) (dashed lines), and Schmidt et al. (1998) (dot-dashed line). The dotted lines were calculated using the equation of state of Duan et al. (1995). L = liquid field, L(40) = liquid containing 40 wt.% NaCl, L + V = coexisting liquid and vapor field, L + H = coexisting liquid and halite field, L + V + H = field of coexisting liquid, vapor, and halite.

increasing temperature. This is probably partly due to the assumption by Duan et al. (1995) that NaCl in solution occurs as an ion-pair over the complete PTX range of their equation, and does not account for the increasingly significant NaCl dissociation with decreasing temperature. Critical points of ternary compositions calculated using the equation of state of Duan et al. (1995) are mostly inconsistent with experimentally determined critical points (Figs. 5 and 6). There are also large differences in the temperatures of halite liquidi between values predicted by the equation of state and the experimental data (Fig. 7). These inconsistencies also occur at the composition H_2O + 40 wt.% NaCl where they cannot be explained by the use of silver oxalate as CO_2 source in the synthetic fluid inclusion experiments. In this study, we showed that the compositional error introduced by using silver oxalate does not have a large effect on iso-Th line slopes and solvus pressures for a bulk composition of H_2O + 10 mol.% CO_2 + 6 wt.% NaCl (Fig. 5c). However, it is presently not known if this statement also holds for more CO_2- and NaCl-rich compositions.

4. SUMMARY

Using the synthetic fluid inclusion technique, dP/dT slopes of iso-Th lines, high-pressure portions of solvi, critical properties, and halite dissolution temperatures in equilibrium with vapor and aqueous liquid were determined for water-rich compositions in the ternary system H_2O-NaCl-CO_2. The previously available database was extended to salinities of 40 wt.% NaCl, compositions up to 20 mol.% CO_2 relative to water, temperatures to 800°C, and pressures to 500 MPa. The experimental results reported here are necessary for the interpretation of natural fluid inclusions and for the development of supercritical water oxidation technology for the treatment of hazardous organic waste.

Addition of NaCl or carbon dioxide, or both, to water has a profound effect on solvus and critical point locations. The obtained data show that immiscibility occurs over a very wide range of PTX conditions and is possible even in deeper crustal rocks. The critical point shifts rapidly to higher pressures and temperatures with rising NaCl and CO_2 concentration. The dP/dT slopes of lines of equal homogenization temperature increase with salinity and carbon dioxide concentration and decrease with homogenization temperature. Both isochore slopes and solvus positions within the (H_2O + 6 wt.% NaCl)-CO_2 pseudobinary are in reasonable agreement with the experimental data of Gehrig (1980). Halite dissolution temperatures in the presence of liquid and vapor show a slight dependence on the carbon dioxide concentration.

Several isoplethic phase diagrams for the system H_2O-NaCl-CO_2 in P-T space have been constructed. These diagrams compare results obtained by researchers who used a variety of experimental techniques with the most recent equation of state for this system by Duan et al. (1995). These data are designed to help petrologists and geochemists to interpret microthermometric data for H_2O-NaCl-CO_2 fluid inclusions and to evaluate the uncertainties in isochore and solvus locations resulting from differences between the experimental datasets and the equation of state.

Acknowledgments—Funding for this research was provided by the Geosciences Program, Office of Basic Energy Sciences, US Department of Energy (DOE) under Grant DE-FG05-89ER14065 to RJB. Funding for the HDAC work was provided by NSF Grant EAR-9725248 to RJB. The authors greatly appreciate the support and contributions by Sarah Beutner, Mark Fortney, Frank Harrison, David Hewitt, John Mavrogenes, Don Rimstidt, Ed Roedder, Kevin Rosso, James Student, and Bob Tracy. I-Ming Chou and Bill Bassett made the analysis of synthetic fluid inclusions using a hydrothermal diamond–anvil cell possible. Matthias Gottschalk provided the program for the calculation of phase equilibria and PVT properties based on the equation of state for H_2O-NaCl-CO_2 fluids of Duan et al. (1995). Reviews by I-Ming Chou, Larryn Diamond, Yves Krüger, and an anonymous reviewer substantially improved the manuscript.

REFERENCES

Anderko A. and Pitzer K. S. (1993) Equation of state representation of phase equilibria and volumetric properties of the system NaCl-H_2O above 573 K. *Geochim. Cosmochim. Acta* **57,** 1657–1680.

Barton P. B. and Chou I-M. (1993) Calculation of the vapor-saturated liquidus for the NaCl-CO_2-H_2O system. *Geochim. Cosmochim. Acta* **57,** 2715–2723.

Bassett W. A., Shen A. H., Bucknum M., and Chou I-M. (1993) A new diamond anvil cell for hydrothermal studies to 2.5 GPa and from −190 to 1200°C. *Rev. Sci. Instrum.* **64,** 2340–2345.

Blencoe J. G., Seitz J. C., Anovitz L. M., Joyce D. B., and Bodnar R. J. (1996) Thermodynamic mixing properties of C-O-H-N fluids at high pressures and temperatures. In *Reactivity and Mobility of Geologic Fluids: Constraints from Inorganic Geochemistry. Symp. ORNL Prog. Abstr.* 10.

Bodnar R. J. (1994) Synthetic fluid inclusions: XII. Experimental determination of the halite liquidus and isochores for a 40 wt.% H_2O-NaCl solution. *Geochim. Cosmochim. Acta* **58,** 1053–1063.

Bodnar R. J. (1995) Applications of synthetic fluid inclusions in supercritical water oxidation research. *Proc. 12th International Conference on the Properties of Water and Steam,* 644–651.

Bodnar R. J. and Costain J. K. (1991) Effect of fluid composition on mass and energy transport in the earth's crust. *Geophys. Res. Lett.* **18,** 983–986.

Bodnar R. J. and Sterner S. M. (1985) Synthetic fluid inclusions in natural quartz. II. Application to PVT studies. *Geochim. Cosmochim. Acta* **49,** 1855–1859.

Bodnar R. J. and Sterner S. M. (1987) Synthetic fluid inclusions. In *Hydrothermal Experimental Techniques* (ed. G. C. Ulmer and H. L. Barnes). pp. 423–457. Wiley.

Bodnar R. J. and Vityk M. O. (1994) Interpretation of microthermometric data for H_2O-NaCl fluid inclusions. In *Fluid Inclusions in Minerals, Methods and Applications* (ed. B. De Vivo and M. L. Frezotti), pp. 117–130. Virginia Tech.

Bodnar R. J., Burnham C. W., and Sterner S. M. (1985) Synthetic fluid inclusions in natural quartz. III. Determination of phase equilibrium properties in the system H_2O-NaCl to 1000°C and 1500 bars. *Geochim. Cosmochim. Acta* **49,** 1861–1873.

Bodnar R. J., Binns P. R., and Hall D. L. (1989) Synthetic fluid inclusions. VI. Quantitative evaluation of the decrepitation behavior of fluid inclusions in quartz at one atmosphere confining pressure. *J. Metam. Geol.* **7,** 229–242.

Bowers T. S. and Helgeson H. C. (1983a) Calculation of the thermodynamic and geochemical consequences of nonideal mixing in the system H_2O-CO_2-NaCl on phase relations in geologic systems: Equation of state for H_2O-CO_2-NaCl fluids at high pressures and temperatures. *Geochim. Cosmochim. Acta* **47,** 1247–1275.

Bowers T. S. and Helgeson H. C. (1983b) Calculation of the thermodynamic and geochemical consequences of nonideal mixing in the system H_2O-CO_2-NaCl on phase relations in geologic systems: Metamorphic equilibria at high pressures and temperatures. *Amer. Mineral.* **68,** 1059–1075.

Bozzo A. T., Chen H-S., Kass J. R., and Barduhn A. J. (1975) The properties of the hydrates of chlorine and carbon dioxide. *Desalination* **16,** 303–320.

Brown P. E. and Lamb W. M. (1989) P-V-T properties of fluids in the system H_2O ± CO_2 ± NaCl: New graphical presentations and implications for fluid inclusion studies. *Geochim. Cosmochim. Acta* **53,** 1209–1221.

Chen H-S. (1972) The thermodynamics and composition of carbon dioxide hydrate. M.Sc. thesis, Syracuse Univ.

Chou I-M. (1988) Halite solubilities in supercritical carbon dioxide-water fluids. *GSA Abstr. Prog.* **20,** A76. (abstr.).

Chou I-M., Shen A. H., and Bassett W. A. (1994) Applications of the hydrothermal diamond-anvil cell in fluid inclusion research. In *Fluid Inclusions in Minerals, Methods and Applications* (ed. B. De Vivo and M. L. Frezotti). pp. 215–230. Virginia Tech.

Darling R. S. (1991) An extended equation to calculate NaCl contents from final clathrate melting temperatures in H_2O-CO_2-NaCl fluid inclusions: Implications for P-T isochore location. *Geochim. Cosmochim. Acta* **55,** 3869–3871.

Diamond L. W. (1992) Stability of CO_2 clathrate hydrate + CO_2 liquid + CO_2 + aqueous KCl-NaCl solutions: Experimental determination and application to salinity estimates of fluid inclusions. *Geochim. Cosmochim. Acta* **56,** 273–280.

Diamond L. W. (1994) Salinity of multivolatile fluid inclusions determined from clathrate hydrate stability. *Geochim. Cosmochim. Acta* **58,** 19–41.

Diamond L. W. (1996) Isochoric paths in immiscible fluids and the interpretation of multicomponent fluid inclusions. *Geochim. Cosmochim. Acta* **60,** 3825–3834.

Drummond S. E., Jr. (1981) Boiling and mixing of hydrothermal fluids: Chemical effects on mineral precipitation. Ph.D. Dissertation, Penn. State Univ.

Duan Zh., Møller N., and Weare J. H. (1995) Equation of state for the NaCl-H_2O-CO_2 system: Prediction of phase equilibria and volumetric properties. *Geochim. Cosmochim. Acta* **59,** 2869–2882.

Ellis A. J. and Golding R. M. (1963) The solubility of carbon dioxide above 100°C in water and in sodium chloride solutions. *Amer. J. Sci.* **261,** 47–60.

Frantz J. D., Zhang Y., Hickmott, D. D., and Hoering T. C. (1989) Hydrothermal reactions involving equilibrium between minerals and mixed volatiles: 1. Techniques for experimentally loading and analyzing gases and their application to synthetic fluid inclusions. *Chem. Geol.* **76,** 57–70.

Frantz J. D., Popp R. K., and Hoering T. C. (1992) The compositional limits of fluid immiscibility in the system H_2O-NaCl-CO_2 as determined with the use of synthetic fluid inclusions in conjunction with mass spectrometry. *Chem. Geol.* **98,** 237–255.

Gehrig M. (1980) Phasengleichgewichte und pVT-Daten ternärer Mischungen aus Wasser, Kohlendioxid und Natriumchlorid bis 3 kbar und 550°C. Doctoral dissertation, Univ. Karlsruhe.

Gibert F., Guillaume D., and Laporte D. (1998) Importance of fluid immiscibility in the H_2O-NaCl-CO_2 system and selective CO_2 entrapment in granulites: Experimental phase diagram at 5–7 kbar, 900°C and wetting textures. *Eur. J. Mineral.* **10,** 1109–1123.

Haar L., Gallagher J. S., and Kell G. S. (1984) *NBS/NRC Steam Tables: Thermodynamic and Transport Properties and Computer Programs for Vapor and Liquid States of Water in SI Units*. Hemisphere Publ. Co.

Hosieni K. R., Howald R. A., and Scanlon M. W. (1985) Thermodynamics of the lambda transition and the equation of state of quartz. *Amer. Mineral.* **70,** 782–793.

Johnson E. L. (1991) Experimentally determined limits for H_2O-CO_2-NaCl immiscibility in granulites. *Geology* **19,** 925–928.

Johnson E. L. (1992) An assessment of the accuracy of isochore location techniques for H_2O-CO_2-NaCl fluids at granulite facies pressure-temperature conditions. *Geochim. Cosmochim. Acta* **56,** 295–302.

Joyce D. B. and Holloway J. R. (1993) An experimental determination of the thermodynamic properties of H_2O-CO_2-NaCl fluids at high pressures and temperatures. *Geochim. Cosmochim. Acta* **57,** 733–746.

Knight C. L. and Bodnar R. J. (1989) Synthetic fluid inclusions: IX. Critical PVTX properties of NaCl-H_2O solutions. *Geochim. Cosmochim. Acta* **53,** 3–8.

Kotelnikov A. R. and Kotelnikova Z. A. (1990) An experimental study of the phase state of the system H_2O-CO_2-NaCl using synthetic fluid inclusions in quartz. *Geokhimiya* **4,** 526–537. (in Russian).

Krüger Y. and Diamond L. W. (in press) Unexpected behaviour of fluid

inclusions synthesized from silver oxalate and an aqueous NaCl solution. *Chem. Geol.*

Labotka T. C. (1991) Chemical and physical properties of fluids. In *Reviews in Mineralogy* (ed. D. M. Kerrick). Vol. 26, pp. 43–104. Mineralogical Society of America.

Lowry H. H. and Erickson W. R. (1927) The densities of coexisting liquid and gaseous carbon dioxide and the solubility of water in liquid carbon dioxide. *J. Amer. Chem. Soc.* **49,** 2729–2734.

Malinin S. D. and Kurovskaya N. A. (1975) Solubility of CO_2 in chloride solutions at elevated temperatures and CO_2 pressures. *Geochem. Intl.* **12,** 199–201.

Malinin S. D. and Savelyeva N. I. (1972) The solubility of CO_2 in NaCl and $CaCl_2$ solutions at 25, 50, and 75° under elevated CO_2 pressures. *Geochem. Intl.* **9,** 410–417.

Pitzer K. S. (1986) Large-scale fluctuations and the critical behavior of dilute NaCl in H_2O. *J. Phys. Chem.* **90,** 1502–1504.

Plyasunova N. V. and Shmulovich K. I. (1991) Phase equilibria in the system H_2O-CO_2-$CaCl_2$ at 500°C. *Transactions (Doklady) USSR Acad. Sci.* **320,** 7, 221–225.

Roedder E. (1984) *Fluid Inclusions. Reviews in Mineralogy Vol.* 12, Mineralogical Society of America.

Schmidt C., Rosso K. M., and Bodnar R. J. (1995) Synthetic fluid inclusions: XIII. Experimental determination of PVT properties in the system H_2O + 40 wt.% NaCl + 5 mol.% CO_2 at elevated temperature and pressure. *Geochim. Cosmochim. Acta* **59,** 3953–3959.

Schmidt C., Chou I-M., Bodnar R. J., and Bassett, W. A. (1998) Microthermometric analyses of synthetic fluid inclusions using the hydrothermal diamond–anvil cell. *Amer. Mineral.* **83,** 995–1007.

Shaw R. W., Brill T. B., Clifford A. A., Eckert C. A., and Franck E. U. (1991) Supercritical water: A medium for chemistry. *Chem. & Eng. News* **69,** no.51., 26–39.

Shen A. H., Bassett W. A., and Chou I-M. (1993) The α-β quartz transition at high temperatures and pressures in a diamond-anvil cell by laser interferometry. *Amer. Mineral.* **78,** 694–698.

Shmulovich K. I. and Graham C. M. (1999) An experimental study of phase equilibria in the system H_2O-CO_2-NaCl at 800°C and 9 kbar. *Contrib. Mineral. Petrol.* **136,** 247–257.

Shmulovich K. I. and Plyasunova N. V. (1993) Phase equilibria in ternary systems formed by H_2O and CO_2 with $CaCl_2$ or NaCl at high P and T. *Geochem. Intl.* **30,** 53–71.

Sourirajan S. and Kennedy G. C. (1962) The system H_2O-NaCl at elevated temperatures and pressures. *Amer. J. Sci.* **260,** 115–141.

Sterner S. M. (1992) Synthetic fluid inclusions. XI. Notes on the application of synthetic fluid inclusions to high P-T experimental aqueous geochemistry. *Amer. Mineral.* **77,** 156–167.

Sterner S. M. and Bodnar R. J. (1984) Synthetic fluid inclusions in natural quartz. I: Compositional types synthesized and applications in experimental geochemistry. *Geochim. Cosmochim. Acta* **48,** 2659–2668.

Sterner S. M. and Bodnar R. J. (1991) Synthetic fluid inclusions. X: Experimental determination of *P-V-T-X* properties in the CO_2-H_2O system to 6 kb and 700°C. *Amer. J. Sci.* **291,** 1–54.

Sterner S. M., Hall D. L., and Bodnar R. J. (1988) Synthetic fluid inclusions. V. Solubility relations in the system NaCl-KCl-H_2O under vapor-saturated conditions. *Geochim. Cosmochim. Acta* **52,** 989–1005.

Takenouchi S. and Kennedy G. C. (1964) The binary system H_2O-CO_2 at high temperatures and pressures. *Amer. J. Sci.* **262,** 1055–1074.

Takenouchi S. and Kennedy G. C. (1965) The solubility of carbon dioxide in NaCl solutions at high temperatures and pressures. *Amer. J. Sci.* **263,** 445–454.

Tester J. W., Holgate H. R., Armellini F. J., Webley P. A., Killilea W. R., Hong G. T., and Barner H. E. (1992) Supercritical water oxidation technology: A review of process development and fundamental research. *1991 ACS Symposium Series: Emerging Technologies for Hazardous Waste Management III,* Atlanta, GA.

Tödheide K. and Franck E. U. (1963) Das Zweiphasengebiet und die kritische Kurve im System Kohlendioxid-Wasser bis zu Drucken von 3500 bar. *Zeitschr. Phys. Chemie Neue Folge* **37,** 387–401.

Werre R. W., Jr., Bodnar R. J., Bethke P. M., and Barton P. B., Jr. (1979) A novel gas-flow fluid inclusion heating/freezing stage. *Geol. Soc. Amer. Abstr. with Prog.* **11**, 539. (abstr.).

Yasunishi A. and Yoshida F. (1979) Solubility of carbon dioxide in aqueous electrolyte solutions. *J. Chem. Eng. Data* **24,** 11–14.